Presynaptic inhibition of cutaneous afferents prevents chronic itch

Augusto Escalante[12*] and Rüdiger Klein[1*]

[1] Department Molecules-Signaling-Development, Max Planck Institute of Neurobiology, Am Klopferspitz 18, 82152 Martinsried, Germany

[2] Current address: Instituto de Neurociencias, Developmental Neurobiology Unit, Campus de San Juan, 03550 San Juan de Alicante, Spain

* Corresponding authors:

Augusto Escalante: aescalante@neuro.mpg.de , aescalante@umh.es

Rüdiger Klein: rklein@neuro.mpg.de

SUMMARY

Chronic itch represents an incapacitating burden on patients suffering a wide spectrum of diseases. Despite recent advances in our understanding of the cells and circuits implicated in the processing of itch information, chronic itch often presents itself without apparent cause. Here, we identify a spinal subpopulation of inhibitory neurons defined by the expression of Ptf1a involved in gating mechanosensory information self-generated during locomotion. These neurons receive tactile and motor input and establish presynaptic inhibitory contacts on mechanosensory afferents. Loss of these neurons leads to increased hairy skin sensitivity and chronic itch, at least partially mediated through the classic GRPR pathway. These findings shed new light on the mechanisms implicated in chronic itch and open novel targets for therapy developments.

Introduction

Itch is defined as an unpleasant sensation that elicits the desire or reflex to scratch (Hafenreffer, 1660). Despite its high prevalence, health and economic burden (Tripathi et al., 2019; Schut et al. 2019; Weisshaar et al., 2019) chronic itch remains a disease without cure and very ineffective treatments to date (Oetjen et al., 2017). Under physiological conditions, chemical itch is initiated by receptors located in the skin, known as pruriceptors, which react to a plethora of chemical substances (Dong and Dong, 2018). On the other hand, mechanical itch is triggered by light tactile stimuli, for example the sensation elicited by an insect crawling across the skin. It is also a widespread symptom associated with many skin and systemic diseases (Yosipovitch and Bernhard, 2013; Mollanazar et al., 2016), but in healthy humans it has only been unequivocally induced under laboratory experimental conditions (Ikoma et al., 2005; Fukuoka et al., 2013). Thus, identifying and understanding the neural circuits that mediate itch responses to mechanical stimuli remains a major challenge.

The spinal cord dorsal horn is the first relay center for itch information. Spinal cord neurons expressing the gastrin releasing peptide receptor (GRPR) are required for itch sensation (Sun and Chen, 2007; Sun et al., 2009). Recently, it was postulated that only chemical but not mechanical itch signals are conveyed through the GRPR pathway. Indeed, it has been shown very recently that dorsal horn neurons expressing the neuropeptide Y1 receptor (NPY1R, Acton et al., 2019) and/or urocortin 3 (UBC3, Pan et al., 2019) transmit exclusively mechanical itch information. However, the nature of the stimulus inducing the spontaneous scratching in these mutant/ablated mice, that leads to developing self-inflicted skin wounds, has remained elusive.

The spinal dorsal horn is under strong inhibitory drive imposed by both local and supraspinal systems (Sorkin and Puig, 1996, 1998). It has long been recognized the importance of maintaining a high level of inhibitory control over incoming somatosensory information in the spinal dorsal horn (Zeilhofer et al., 2012; Bardoni et al., 2013). Among inhibitory systems, spinal presynaptic inhibition has been shown to play a fundamental role in modulating various types of sensory afferents (Rudomin and Schmidt, 1999; Rudomin, 2009; Fink et al., 2014; Azim et al., 2014; Zimmerman et al., 2019). Inhibition at the terminals of sensory afferents allows for the reduction in excitability of downstream neurons without postsynaptic inhibition of the target neurons themselves. Presynaptic inhibition is thought to reduce gain at sensory synapses and filter out irrelevant or self-generated sensory cues in order to preserve the ability to generate adequate responses to environmental stimuli in many animal species (Watson, 1992; Frost et al., 2003; Seki et al., 2003; Poulet and Hedwig, 2006). In the spinal dorsal horn, inhibitory interneurons named GABApre neurons, characterized by expression of Pancreas transcription factor 1a (Ptf1a), were identified as the source of presynaptic inhibitory synapses onto ventral proprioceptive and dorsal cutaneous afferents (Betley et al., 2009). GABApre neurons-mediated presynaptic inhibition was shown to control proprioceptive input to regulate fine motor tasks (Fink et al., 2014).

During the last few years, several studies have identified populations of dorsal horn spinal inhibitory neurons involved in processing of somatosensory information (Duan et al., 2014; Petitjean et al., 2015; Cui et al., 2016; Koch et al., 2017; Koch et al., 2018; Francois et al., 2017). Several of these studies described the development of spontaneous scratching behavior after

loss of some partially overlapping populations of inhibitory neurons. These mice developed a heightened itch sensitivity to chemical (Ross et al., 2010; Foster et al., 2015) or mechanical (Bourane et al., 2015) stimulation. These inhibitory neurons also share a common developmental origin. Spinal dorsal inhibitory neurons derive from the dIL4/dILA class of interneurons defined during spinal cord neurogenesis through selective expression of defined transcription factor combinations (Gross et al., 2002; Müller et al., 2002; Helms and Johnson, 2003; Cheng et al., 2004; Cheng et al., 2005; Mizuguchi et al., 2006; Wildner et al., 2006). Ptf1a is transiently expressed in neural progenitors and acts as the main selector gene in establishing the dIL4/dILA class (Glasgow et al., 2005). Specifically, it has been shown that Ptf1a is required for the specification of the subpopulations of inhibitory neurons implicated in itch processing: dynorphin (Huang et al., 2008; Wildner et al., 2013), glycinergic transporter 2 (Huang et al., 2008; Wildner et al., 2013; Borromeo et al., 2014) and neuropeptide Y (Huang et al., 2008; Bröhl et al., 2008; Wildner et al., 2013) positive neurons.

According to these studies, there seems to be a common link between spinal inhibitory neurons responsible for presynaptic inhibition in the dorsal horn and subpopulations of inhibitory neurons demonstrated to play a role in the gating of somatosensory information whose loss leads to the development of chronic itch. Here, we have used this link, Ptf1a, as a genetic entry point for manipulating these subpopulations at once in mice and assessing their role in itch behavior. Our findings indicate that Ptf1a-derived inhibitory interneurons are essential components of a gating mechanism designed to block incoming self-generated mechanosensory information. Selective elimination of these neurons through intersectional genetics leads to the development of the highest frequency spontaneous scratching behavior described to date. We find that no other somatosensory modalities, including chemical itch, are affected and gross motor behavior remained unchanged. These mice present increased hairy skin sensitivity and, following long-term video analysis in their own home cage, we show that scratching phenotype is dependent on the level of activity of the animals. Finally, we show that GRPR at least partially mediate Ptf1a-ablated animals scratching phenotype and that Ptf1a-derived interneurons control GRPR-mediated itch. These results argue for Ptf1a as a common determinant of inhibitory neuron populations blocking irrelevant mechanosensory input into spinal dorsal horn and postulate chronic spontaneous scratching as a consequence of excessive entry of innocuous tactile information.

Results

Ptf1a-derived neurons make for most but not all inhibitory neurons in the dorsal horns

To begin to test the hypothesis that Ptf1a-derived neurons constitute a subpopulation of spinal inhibitory neurons gating mechanosensory information, we first analyzed the two Cre recombinase knock-in mouse lines available: Ptf1a::Cre^{CVW} (Kawaguchi et al., 2002) and Ptf1a::Cre^{EX1} (Nakhai et al., 2007), hereafter referred to as Ptf1a^{CVW} and Ptf1a^{EX1}, respectively. Even though Ptf1a^{CVW} has been extensively characterized in previous studies (Glasgow et al., 2005; Guo et al., 2012; Meredith et al., 2009; Wildner et al., 2013; Comer et al., 2015; Mona et al., 2017), it is recognized that recombination efficiency is low in this mouse line (Glasgow et al.,

2005; Betley et al., 2009). Given that, we pursued to compare this mouse line with another knock-in mouse line of Ptf1a, Ptf1a^{EX1}, in the expectation that it would present a better efficiency of recombination allowing access to a wider set of the Ptf1a-derived spinal neurons. In the spinal dorsal horns of adult Ptf1a^{CVW} and Ptf1a^{EX1} carrying the Ai9$^{lsl\text{-}tdTomato}$ reporter (Madisen et al., 2010), Ptf1a-derived cells were 2-fold more abundant in the Ptf1a^{EX1} than in the Ptf1a^{CVW} mouse line (Figure 1A and Figure S1A-B). As a reference, dorsal horn excitatory neurons labelled with Lmx1b::Cre (Li et al., 2010; Alaynick et al. 2011) were in turn 2-fold more abundant than Ptf1a^{EX1} derived neurons using the same reporter mouse line (Figure 1A and Figure S1C). Thus, given the higher level of recombination efficiency, we continued our research using the Ptf1a^{EX1} mouse line.

Since Ptf1a^{EX1} has been mostly used for studies in pancreas, we fate mapped Ptf1a^{EX1} derived neurons in the spinal cord throughout development in order to obtain a better idea of the distribution and contribution to the adult dorsal horns. We observed the expected (observed previously for Ptf1a^{CVW}: Glasgow et al., 2005; Meredith et al., 2009) pattern of neurons originating from the mid-dorsal progenitor domain, following mediolateral migration of postmitotic neurons and accumulation in the lateral early alar plates (Figure 1B-D). These neurons constitute the dI4/dILA class of spinal neurons (REFs). A subset of early Ptf1a-derived neurons migrated ventrally towards the floor plate (Figure 1B-D), however very few neurons were found occupying ventral locations in the mature spinal cord (Figure 1E-F). For comparison we performed the same fate mapping study of excitatory dI5/dILB neurons labelled by Lmxb1^{Cre} and found a very similar pattern of migration of early born neurons that subsequently are not found in ventral domains of the adult spinal cord (Figure S1D-H).

In keeping with this analysis, we analyzed the same mouse line used to ablate Ptf1a-derived neurons, Tau$^{ds\text{-}DTR}$ (Duan et al., 2014; see below), to further characterize the distribution and colocalization of adult Ptf1a neurons in the dorsal horns. We took advantage of the nuclear expression of β-galactosidase (β-gal) in Cre expressing cells of this mouse line to label Ptf1a^{EX1} neurons (Figure 2A). β-gal positive neurons were found in the dorsal horn, with the majority of them located more than 200 µm dorsal from the central canal (Figure 2B-C). This distribution followed the same pattern as that of Pax2 expressing cells, a well-accepted marker of inhibitory neurons in the spinal cord (Punnakkal et al., 2014) (Figure 2D-E). The distribution map of co-labelled neurons expressing β-gal and Pax2 shows the same features as that of the two parent populations but it also shows that even if the majority of Pax2^{+} neurons are also β-gal^{+}, there is still a ~22% of Pax^{+} neurons that do not derive from the Ptf1a^{EX1} lineage (Pax2^{+} β-gal^{+}/ Pax2^{+}) (Figure 2F-H).

Adult dorsal horn presynaptic inhibitory neurons receive mechanosensory and motor input.

The Ptf1a lineage gives rise to the population of inhibitory neurons that control proprioceptive and cutaneous somatosensory afferents presynaptically, named GABApre neurons (Betley et al., 2009; Russ et al., 2013; Fink et al., 2014; Ashrafi et al., 2014; Mende et al., 2016; Zhang et al., 2017). To measure the prevalence of Ptf1a-derived neurons among the GABApre subtype in the adult spinal cord, Ptf1a^{EX1} mice carrying the Tau$^{lsl\text{-}SynaptophysinGFP}$ allele (Tripodi et al., 2011) (Figure

2I) were immunohistochemically assessed. SynapthophysinGFP signal in thoracic sections of adult spinal cords was most abundant in the dorsal horns (Figure 2J). Next, we quantified the co-localization of GFP to inhibitory vGAT+ puncta presynaptic to vGlut1+, expressed in large-diameter sensory afferent terminals (Orefice et al., 2016; Abraira et al., 2017) (Figure 2K and S2A) in the upper dorsal horn. More than 80% of presynaptic inhibitory contacts on vGlut1+ sensory terminals derive from Ptf1a^{EX1} neurons (Figure S2B), confirming previous analysis performed during early postnatal stages (Betley et al., 2009).

To gain further insights into the type of monosynaptic inputs received by Ptf1a^{EX1} neurons, we performed retrograde transneuronal tracing with EnvA-pseudotyped G-deleted-GFP rabies virus (SADΔG-GFP) (Wickersham et al., 2006) using a genetic approach. Ptf1a^{EX1} mice crossed to RΦGT (Takatoh et al, 2013) express the auxiliary TVA and G proteins only in Cre neurons (Figure 2L) directing specific infection of SADΔG-GFP to Ptf1a^{EX1} neurons. Injections were performed in adult animals and analyzed 6 days later. We found numerous GFP neurons in 5-6 adjacent DRGs ipsilateral to the injection site (Figure 2L). Immunohistochemical characterization of DRG GFP$^+$ neurons (Figure 2M-N) showed that most of the sensory neurons establishing direct synapses with Ptf1a^{EX1} neurons are low threshold mechanoreceptors (LTMRs) involved in transmission of touch information: NF200$^+$ (32.04±4.26%), NF200$^+$CGRP$^+$ (43.73±6.85%), TrkC$^+$ (12.76±0.81%), TH$^+$ (8.86±8.04%). A small percentage of them were associated with unmyelinated peptidergic nociceptive neurons: CGRP$^+$NF200$^-$ (12.6±7.07), very few with proprioceptive inputs: PV$^+$ (2.12±0.5%) and PV$^+$TrkC$^+$ (1.06±0.63) and none with non-peptidergic nociceptors (IB4$^+$) (Lallemend and Ernfors, 2012; Bourane et al., 2015b; Usoskin et al., 2015).

We also observed that Ptf1a^{EX1} neurons receive monosynaptic inputs from supraspinal regions, most of which have been associated with descending motor pathways (Figure 2O-P). The most prominent regions with direct inputs to Ptf1a^{EX1} neurons were the motor cortex (32.95±12%), where GFP+ neurons were located in layer V, corresponding to corticospinal projection neurons known to be involved in skilled movements (Moreno-Lopez et al, 2016; Ueno et al., 2018) and the gigantocellular nucleus (Gi) (30.1±12.33%), part of the reticulospinal tract that has been described to be important in motor control (Bouvier et al., 2015; Liang et al., 2016; Capelli et al., 2017; Brownstone and Chopek, 2018). The next most abundant regions with inputs to Ptf1a^{EX1} neurons were the red nucleus (4.56±1.6%), the medullary reticular nucleus (4.02±0.92%) and the raphe (3.92±2.86%) (Figure 2Q). Thus, Ptf1a^{EX1} neurons receive direct mechanosensory and higher motor information.

Ablation of Ptf1a^{EX1} spinal neurons leads to a loss of dorsal GABApre neurons

To begin to functionally characterize Ptf1a^{EX1} neurons, we selectively ablated Ptf1a^{EX1} neurons in the adult spinal cord using an intersectional genetic approach. Combination of Ptf1a^{EX1} with a mouse line expressing Flp caudal to C5 region of the mouse embryo, Cdx2^{FlpO} (Britz et al., 2015), allows restriction of the human diphtheria toxin receptor (DTR) to spinal neurons expressing both Cre and FlpO in the Tau$^{ds\text{-}DTR}$ efector line (Figure 3A). Adult ablation was achieved through the administration of diphtheria toxin (DTx) to double recombinase positive animals at 7-8 weeks of

age. Littermates lacking one of the recombinase alleles but carrying the Tau$^{ds\text{-}DTR}$ allele were used as controls and received the same dosage of DTx.

First, we tested that Cdx2^{FlpO} was efficient in combination with Ptf1a^{EX1}. Spinal cords of mice carrying the three alleles Ptf1a^{EX1};Cdx2^{FlpO};Ai9^{lsltdTomato} show loss of tdTomato fluorescence, due to the removal of the whole FRT-flanked Ai9 cassette (Madisen et al., 2010), caudally to spinal segment C5 (Figure S3A-C). We also tested Ptf1a^{EX1};Cdx2^{FlpO} in combination with Tau$^{ds\text{-}DTR}$ for the loss of β-gal expression in Ptf1a^{EX1} neurons in the presence of Cdx2^{FlpO} (Figure S3D-E), demonstrating the efficiency of the system to specifically target Ptf1a^{EX1} in the spinal cord.

Based on the Ai65D$^{ds\text{-}tdTomato}$ Cre- and Flp-dependent tdTomato reporter allele (Madisen et al., 2015), 40% of Ptf1a^{EX1} neurons were ablated in the thoracic spinal cord (Figure 3B-D). Compared to a reduction in the number of Pax2^{+} dorsal spinal neurons of 36% (Figure3E-G), these numbers show that out of the 77% of Pax2 neurons derived from the Ptf1a^{EX1} lineage, we roughly target half of them. DTx ablation seemed to differentially affect Ptf1a^{EX1} neurons given that the spatial distribution of Pax2+ cells changed medio-ventrally comparing control to Ptf1a-ablated animals: median position shifted 52 µm ventrally and 41 µm medially (Figure 3H and S3F). Possibly indicating a bias in the DTx sensitivity previously observed with other combinations of Cre and Flp mouse lines (Duan et al., 2014; Huang et al., 2019). On the other hand, neither numbers nor distribution of excitatory dorsal horn neurons assessed by expression of Lmx1b were affected upon DTx treatment (Figure S3F-I). Also unaffected were terminals of non-peptidergic nociceptors marked with IB4, sensory terminals of Aβ and Aδ fibers marked by vGlut1 and excitatory terminals marked with vGlut2 (Figure S3N-P). Other markers of spinal inhibitory neurons were also unaffected by Ptf1a^{EX1} ablation: Enkephalin, Galanin, nNOS (Figure S3J-M). Remarkably no difference was found on the expression of NPY (Figure 3I-K), indicating that DTx-mediated ablation through Ptf1a^{EX1} was differentially targeting only a subset of inhibitory neurons.

In order to estimate the effect of ablating Ptf1a^{EX1} neurons on the GABApre neuron subtype, we measured the expression of GAD65, a marker of GABApre presynaptic terminals in the spinal dorsal horn (Hughes et al., 2005; Betley et al., 2009; Mende et al., 2016) of control and Ptf1a ablated animals. We focused in the upper laminae to avoid the medioventral part of the dorsal horns where GABApre neurons targeting proprioceptive and not cutaneous afferents are located (Hughes et al, 2005; Zhang et al., 2017). GAD65 expression was decreased 24% (Figure 3L-N). To gain further insights and in the absence of a reporter for Ptf1a^{EX1} terminals, we next quantified the percentage of vGlut1^{+} sensory terminals that received vGAT^{+} contacts among vGlut1^{+} terminals in the upper dorsal horn, assuming that we would underestimate the results given that not every presynaptic inhibitory puncta derives from Ptf1a^{EX1} neurons (see above). Ptf1a-ablated animal dorsal horns have a significant reduction of 18% in the number of presynaptic inhibitory contacts over cutaneous vGlut1 sensory terminals compared to control animals (Figure 3O).

Ptf1a^{EX1} neuron loss leads to increased hairy skin sensitivity and spontaneous scratching

We hypothesized that the spontaneous scratching phenotype observed previously after loss of several inhibitory populations of dorsal horn neurons (Ross et al., 2010; Foster et al., 2015;

Bourane et al., 2015) was due to the reduction in presynaptic inhibition over the mechanosensory input arrival to the dorsal horns. Ptf1a^{EX1} would serve to specifically target GABApre neurons in the upper part of the dorsal horn as we have seen previously and gain a further understanding on the mechanisms and type of stimulus that triggers such aversive behavior. In order to capture the evolution in time of the expected scratching phenotype and to gain a better understanding of such changes in the "natural" environment of laboratory mice, we setup to video record a first cohort of animals before and every day after DTx administration in their own home cages (Figure 4A-B, see Materials and Methods for details).

Ptf1a-ablated animals developed a very intense itch sensation and started to scratch only 2 days after the end of DTx administration (Day 5 since the beginning of the experiment) and reached peak scratching frequency just one day later, scratching 20-fold more than their control littermates. One day more into the experiment scratching frequency stayed at the same values (Day 7) (Figure 4C) but animals started to develop fur loss and skin injuries so experiment was terminated. Scratching was mostly directed to the nape of the neck, the forearm and flanks. Very rarely we observed scratching towards the cheeks, snout or scalp, in accordance with the limitation in spinal rostral ablation imposed by the use of Cdx2^{FlpO} which spares segments receiving somatosensory information from those dermatomes (Takahashi et al., 1992). Hereafter, we grouped results in two categories: PreDT, before DTx treatment (baseline scratch) and PostDT, after DTx treatment (increase of more than 10-fold in scratching in 24 hours). Ptf1a-ablated animals scratched more than 60-fold compared to control littermates after DTx treatment (Figure 4D) and such behavior developed very quickly, reaching peak values 3-6 days after DTx administration (Figure 4E) in average at 6.8 days. We also quantified the grooming time and found that Ptf1a-ablated animals spent 5-fold more time grooming than their control littermates after DTx treatment. Taken together, these findings support the idea of Ptf1a^{EX1} targeting a population of inhibitory neurons mediating itch control in the dorsal horn.

The spontaneous scratching phenotype was not related to chemical itch, as injection of chemical pruritogens in the back region of Ptf1a-ablated animals before the onset of spontaneous scratching -but after loss of Ptf1a^{EX1} neurons (Figure S4A)- showed no differences compared to control littermates (Figure 4G-H). Additional behavioral tests revealed no changes in the processing of other somatosensory modalities (Figure S4B-F), acute mechanical itch (Figure S4G-H), locomotor coordination (Figure S4I-J) and anxiety (Figure S4J). To shed some light on the type of stimuli initiating the itch-scratch cycle in Ptf1a-ablated mice, we studied the scratch response of mice at peak scratching phase before and after removal of bedding material from the home cage. Ptf1a-ablated animals decreased 40% in scratching frequency while no change was observed in control littermates (Figure 4I) indicating a role for the mechanosensory stimuli present in the environment of the animal in the induction of itch. We reasoned that mechanosensory stimuli causing the scratch phenotype might be detected by hairs, the most common mechanoreceptor, in hairy skin since glabrous skin did not show any behavioral defect and designed an experiment to test hairy skin sensitivity to air puffs of different intensities directed towards the back of the animal (Orefice et al., 2016). First, we evaluated the response curve to air puffs of increasing intensities for control animals treated with DTx (Figure S4K). Intensities above 0.1 PSI elicited a significant response compared to mock air puffs at 0.05 PSI. Ptf1a-ablated animals showed a 2-fold increased response to threshold intensity (0.5 PSI) compared to

controls (Control 37.71±2.81 vs Ablated 81.4±15.27 mV) (Figure 4J). Interestingly, ablation of Ptf1a^{EX1} neurons did not alter startle responses or pre-pulse inhibition characteristics in both the acoustic and tactile versions (Orefice et al., 2016) of the assay (Figure S4L-Q).

According to these findings, ablation of Ptf1a^{EX1} neurons leads to heightened hairy skin sensitivity and intense spontaneous scratching that, consequently, depends on the abundance of mechanosensory cues in the environment. In an attempt to establish a causal relationship between hairy skin sensitivity and dorsal horn neuronal activity, we counted the numbers cFos^{+} neurons in the dorsal horns of control and Ptf1a-ablated animals (Figure 4K). Ablation of Ptf1a^{EX1} neurons increased more than 3 times the number of cFos^{+} cells in the dorsal horns (Figure 4L). However, given that this increase in dorsal horn activity could not be attributed to the sensation of the itchy stimulus *per se* alone but to the scratching response as well, we designed a back hair stimulation protocol under anesthesia (Figure 4M). Spinal cords of Ptf1a-ablated animals whose back hair had been stimulated showed (Figure 4N-O) a localized increase of cFos^{+} neurons in the dorsal horns (Figure 4P) almost 4-fold higher than in control animals. As an internal control, the number of cFos^{+} neurons in the ventral spinal cord, a region not innervated by cutaneous afferents, was not altered (Figure 4Q-R). These results support the idea that the spontaneous scratching phenotype observed in Ptf1a-ablated animals is a response to hair self-stimulation that is inhibited by Ptf1a^{EX1} neurons under physiological conditions.

Locomotor activity induces spontaneous scratching in Ptf1a^{EX1}-ablated animals

In the pursuit of understanding the scratching behavior of Ptf1a-ablated animals in a naturalistic as possible environment for laboratory mice (Babayan and Konen, 2019), we designed and built a system to video record individual mice in their own home cages continuously for several days without human interaction (Figure 5A and Material and Methods section). A combination of machine learning methods was used to extract the frames in which the animal performed scratching behavior and analyze the resulting data (Figure S5A). Our aim was to understand if there were differences in the intensity of the phenotype depending on the circadian phase and how we could explain the association between hairy skin and scratching.

We obtained recordings from 6 control and 7 Ptf1a-ablated animals for ca. 90 hours (Figure S5D). The level of activity, measured as locomotion speed, of the animals during the dark phase of the circadian cycle oscillated accordingly with the changes in lightning (Figure 5B). Time spent scratching steadily increased from the second dark phase (equivalent to Day 6 in Figure 4C). Analysis of the time spent scratching during consecutive phases demonstrated that unperturbed Ptf1a-ablated animals scratched more than control during the third light phase (Figure 5C) as previously observed for Day 6. Indeed, analysis of the mice individual scratching behaviors during light and dark phase indicate that the same animals tend to scratch more during the dark phase, than the light phase (Figure 5D-E). This holds true for both control and Ptf1a-ablated animals (Figure S5E-F) which in average scratch more during the dark compared to the light phases (Figure 5F). A similar analysis for the speed of these animals revealed the expected oscillatory pattern with higher average speed during the dark phases and lower speed during the light phases (Figure S5G-I and Figure 5G).

These findings led us to postulate a link between the level of locomotor activity of the animal and the intensity of the scratching phenotype since movement of the animal unescapably would lead to self-activation of its own hairs. A clear correlation between both variables was observed for control animals (Figure 5H) and to a lesser extent for Ptf1a-ablated animals (Figure 5I), probably due to the mandatory reduction in speed imposed by the scratching action. In order to investigate a direct relationship between animal locomotor activity and spontaneous scratching, we evaluated the scratching frequency of the same animals at peak scratching in two different contexts: as previously performed in their own home cage (as per Figure 4) and 30 minutes later in their own home cage once returned to its stabulation rack. Ptf1a-ablated animals in the first context scratched several times more often than control animals as expected, while in the second experiment the same animals reduced scratching frequency 4-fold (Figure 5J). Control animals also reduced scratching in a significant manner. Each individual animal tested decreased its scratching frequency in the second context (Figure 5K). These results are in agreement with the described behavior in the long-term analysis presented above, however, it is possible that higher scratching in the first context was due to an increased anxiety given that in this setting both the cage lid and food tray are removed to have a clear top view of the cage. To rule out this hypothesis, namely that increased scratching frequency is a consequence of increased anxiety and not a consequence of higher locomotor activity, we performed a similar experiment by placing mice in the same holding cylinder used for air puff delivery (as per Figure 4J) to which they were shortly acclimated one day earlier, arguably a context with higher anxiety potential than in the previous experiment. Ptf1a-ablated animals reduced scratching behavior more than 60-fold when placed in the cylinder, a context in which they can still move but not locomote freely (Figure 5L-M). Taken together, these results argue in favor of the idea that spontaneous scratching observed after Ptf1a^{EX1} neuron ablation is an exacerbated response to self-stimulation of fur produced during mice normal locomotion.

GRPR^{+} neurons mediate several aspects of Ptf1a^{EX1}-ablated mice behavior

To figure out the itch circuits involved in the scratching phenotype of Ptf1a-ablated animals, we performed a pilot study to further reduce scratching frequency in Ptf1a-ablated animals by use of a GRPR specific antagonist. Administration of the antagonist reduced 50% the scratching frequency of Ptf1a-ablated animals (Figure S6A). Following this observation and given the importance of spinal GRPR^{+} neurons in itch sensation, we characterized the behavior of GRPR-ablated animals by applying the same intersectional approach used for Ptf1a^{EX1} animals (Figure 6A). Ablation efficiency was low (Figure S6B-D) but GRPR-ablated animals showed a marked decrease in scratching in response to chemical pruritogens (Figure 6B-C). Further behavioral testing indicated no significant differences between control and GRPR-ablated animals (Figure S6E-R) as previously reported for GRPR knockout and saporin-mediated ablation mice (Sun and Chen, 2007; Sun et al., 2009).

To examine whether Ptf1a^{EX1} neurons gate mechanosensory information input to GRPR-mediated itch circuits, we generated triple-recombinase mice carrying the Ptf1a^{EX1}, GRPR^{iCRE} and Cdx2^{FlpO} alleles together with the effector allele Tau$^{ds\text{-}DTR}$ (Figure 6D). Simultaneous ablation of Ptf1a^{EX1} and GRPR neurons did not change the peak scratching frequency of ablated animals

(Figure 6E) but delayed its development by more than one day (Figure 6F). Double-ablated animals also showed a normal response in the hairy skin sensitivity test (Figure 6G). In summary, these results suggest that Ptf1a^{EX1} neurons gate mechanosensory information in the GRPR pathway and that GRPR neurons elicit itch in response to this type of somatosensory input.

Ptf1a^{EX1} neurons inhibit GRPR-mediated itch

To assess the function of Ptf1a^{EX1} neurons using a gain-of-function intersectional approach, we acutely activated Ptf1a^{EX1} neurons with the activating DREADD receptor hM3Dq (Sciolino et al., 2016) (Figure 7A and S7A-B). As previously, we used littermates lacking one of the recombinase alleles treated with clozapine-N-oxide (CNO) as control animals.

In order to assess whether Ptf1a^{EX1} neuronal activation would represent a negative emotional or cognitive valence for mice, we performed a conditioned place aversion assay (CPA). Since most animals initially preferred (IP) one of the CPA chambers, we paired the IP chamber with CNO administration and the initially non-preferred (INP) chamber with vehicle to test whether activation of Ptf1a^{EX1} neurons would decrease or switch the initial preference (Vrontou et al., 2013). On test day, neither control nor Ptf1a-activated animals showed any change in preference (FigureS7C). In line with this result, we did not observe any changes in somatosensory or motor tests after activation of Ptf1a^{EX1} neurons inhibitory neurons (Figure S7D-J).

Analysis of scratching frequency on Ptf1a-activated animals did not reveal any difference after CNO treatment or compared to controls (Figure7C). This result was expected given the low scratching frequency of healthy wild-type mice under laboratory conditions. To test the role of Ptf1a^{EX1} neurons in mechanosensory information gating, we generated a condition of increased itch sensation by activating GRPR neurons using the same intersectional approach (Figure S7K-L). CNO-mediated activation of GRPR neurons induces 20-fold scratching increase compared to vehicle-treated animals (Figure 7C), as recently reported using a different approach (Bardoni et al., 2018). Simultaneous activation of Ptf1a^{EX1} and GRPR neurons in the same animal (Figure 7B), resulted in a 70% reduction in scratching compared to GRPR-activated animals (Figure 7C). Together, these findings indicate that Ptf1a^{EX1} neurons gate mechanosensory information in the GRPR itch circuit.

Activation of GRPR neurons not only resulted in increased itch but also a drastic increase in grooming behavior. GRPR-activated animals spent 80% of the assay time grooming, compared to vehicle treatment that resulted in 23% of time grooming (Figure 7D). Surprisingly, we observed that control animals under CNO treatment groomed significantly more when compared to vehicle treatment (30% vs 18% of the time, respectively) (Figure 7D). We assessed also the grooming behavior of Ptf1a-activated animals and found that even though activation of Ptf1a^{EX1} neurons could inhibit CNO-induced grooming in controls, GRPR-induced grooming was unaffected by simultaneous co-activation of Ptf1a^{EX1} neurons. In summary, our results suggest a well-defined function for Ptf1a^{EX1} neurons in gating specific mechanosensory input to the GRPR itch circuit.

Discussion

Chronic itch is a very common disease and secondary symptom originated from very different causes (from dermatological to oncogenic) that remains without cure nowadays. Treatments are lacking and burden for the patient and society is comparable to that of chronic pain (Kini et al., 2011). In this study, we report that spinal presynaptic inhibitory neurons marked by the expression of the transcription factor Ptf1a gate self-generated mechanosensory information during locomotion to prevent innocuous stimuli from triggering a scratch response. Loss of these neurons gives rise to a chronic itch phenotype and hairy skin hypersensitivity. We propose that presynaptic inhibition of cutaneous afferents in the spinal dorsal horn normally silences self-produced hair activation to facilitate adequate responses to external stimuli.

Common developmental origin of spinal inhibitory neurons gating itch circuits

Our findings shed light on the complex specification of inhibitory neurons in the spinal cord. Ptf1a acts as a selector gene to promote a spinal inhibitory fate and Ptf1a knockout mice lack GABAergic neurons in the dorsal horns (Glasgow et al., 2005). However, Ptf1a knockout mice die perinatally (Glasgow et al., 2005; Hori et al., 2008) precluding any conclusions regarding neuronal subtype composition of the mature dorsal horns.

Previous work identified GAD65, GLYT2 and NPY as adult spinal inhibitory neurons subtypes whose ablation leads to the development of spontaneous scratching (Fink et al., 2014; Foster et al., 2015; Bourane et al., 2015). Each of these genes have been shown to require Ptf1a for proper expression in the dorsal horns during spinal neurogenesis (Huang et al., 2008; Wildner et al., 2013; Borromeo et al., 2014). Such dependency establishes a developmental link for these subtypes to the dIL4/dILA class of inhibitory neurons (Gross et al 2002, Muller et al 2002, Cheng et al 2004, Glasgow et al 2005, Wildner et al 2006). We reasoned that a common specification pathway during development might be relevant for their function in the mature dorsal horn circuits. Indeed, all three genes have been identified as markers for presynaptic inhibitory neurons: GAD65 is believed to be important for these neurons to sustain a high inhibitory tone (Hughes et al., 2005; Betley et al., 2009; Fink et al., 2014) and GLYT2 and NPY are markers for presynaptic inhibitory neurons targeting cutaneous afferents (Betley et al., 2009). Sharing such characteristics, we hypothesized that using Ptf1a as a genetic entry point to manipulate the function of these inhibitory neurons together would reveal the mechanisms of presynaptic inhibition control over the itch response.

Here we used a Ptf1a Cre-knockin mouse line, Ptf1a^{EX1} (Nakhai et al., 2007), with better recombination efficiency than the line most commonly used in spinal cord studies, Ptf1a^{CVW} (Kawaguchi et al., 2002). This is the first time that Ptf1a^{EX1} is used to target spinal neurons. Our results show that Ptf1a^{EX1} targets ~77% of inhibitory neurons expressing Pax2 and several of the well-known markers of spinal inhibitory neurons, including enkephalin, galanin or NPY, are not affected after Ptf1a-ablation. Recent single cell transcriptomic studies of spinal cord neural subtypes during development (Delile et al., 2019), might help solve this puzzle: the authors show at least 6 subtypes of dI4/dILA neurons in the developing spinal cord and only one of them is characterized by the expression of Ptf1a mRNA, whose levels are very low on the other 5 subtypes. Strikingly, NPY appears as a marker of a different subtype. It remains a matter of study

the contribution of Ptf1a protein levels to the specification of different inhibitory subtypes in the spinal cord. Lack of such regulation in Cre-knockin mouse lines could potentially explain these discrepancies.

As shown in our deep behavioral analysis of ablation, loss of Ptf1a^{EX1} neurons results in the most intense spontaneous scratching phenotype reported to date (Ptf1a^{EX1} ablation: 22 bouts/minute, GAD65 ablation: 5 bouts/minute, NPY ablation: 4.2 bouts/minute) and also the fastest to appear after DTx treatment (Ptf1a^{EX1}: 3.7 days, GAD65: 7 days (estimated), NPY: 2 weeks). Our results seem to indicate that Ptf1a^{EX1} captures a more complete set of the inhibitory subtypes involved in mechanical itch gating, resulting in a stronger phenotype. It also emphasizes the importance of presynaptic inhibitory neurons as an essential part of the cutaneous mechanosensory gating mechanisms that impinge onto spinal itch circuits.

Presynaptic inhibition gates self-generated mechanosensory information

Our results showing that Ptf1a^{EX1} neurons make up for more than 80% of all presynaptic inhibitory contacts onto cutaneous mechanosensory fibers in the adult dorsal horns are supported by previous studies that characterized postnatally the developmental origin of spinal presynaptic inhibitory neurons (Betley et al., 2009) and their role in motor control gain (Fink et al., 2014). Presynaptic inhibition at the spinal cord level is a fundamental mechanism for the correct development of tactile sensitivity and adult social interactions among others (Orefice et al., 2016). A recent study explored spinal presynaptic inhibition in depth and elaborated on the importance of this form of sensory input control in hairy skin sensitivity (Zimmerman et al., 2019). Strikingly, the link between both areas of studies, namely Ptf1a^{EX1} neurons, the neurons responsible for such presynaptic inhibition at both types of somatosensory afferents, have been so far missed. Here we show that loss of Ptf1a^{EX1} neurons increases hairy skin sensitivity which leads to the development of a dramatic spontaneous scratching phenotype including severe skin lesions. A careful analysis of such phenotype, which was performed in as naturalistic environment (Datta et al., 2019) as possible for laboratory mice, their own home cages, indicates that loss of presynaptic inhibition onto mechanosensory cutaneous afferents underlies the increased hairy skin sensitivity that ultimately gives rise to scratching. The positive correlation of animal activity with scratching frequency and that of hair stimulation with increased dorsal horn neural activity suggest that self-generated activation of hair mechanosensory inputs during locomotion triggers an exacerbated scratch response in the absence of Ptf1a^{EX1} neurons inhibition. Lack of an acute mechanical itch phenotype as the one previously described for NPY-ablated animals (Bourane et al., 2015; Acton et al., 2019; Pan et al., 2019) agrees with our Ptf1a^{EX1} targeting data, which reveals unaffected expression of NPY in the dorsal horns of Ptf1a-ablated animals. These results point to diverse subsets of presynaptic inhibitory neurons specialized in the gating of different mechanosensory information submodalities.

Thus, Ptf1a^{EX1} neurons seem to be part of a system in charge of blocking self-generated somatosensory stimuli during ongoing motor activity. Such a system has been shown to receive higher motor commands to reduce somatosensory gain during planning and execution of limb movements (Chapman and Tremblay, 2015; Juravle et al., 2017; Voudouris and Fiehler, 2017).

Even though, throughout this work, we have used the term “spontaneous” scratching out of consistency with previous studies, we believe this scratching behavior should be redefined in order to avoid unnecessary confusion and given the existence of a stimulus to which the animal reacts, even if self-generated. We propose the use of “self-induced” scratching behavior, as a possible alternative.

Itch and the perception of tactile stimulation

Our discovery that DREADD-mediated activation of spinal GRPR neurons leads to increased scratching and grooming together with a delayed appearance of scratching phenotype in the simultaneous Ptf1a^{EX1} and GRPR neurons ablation paradigm, begs the question about the connection between itch and innocuous tactile information processing. Previous studies reported no changes in response to acute mechanical itch stimuli presented to GRPR-ablated mice (Bourane et al., 2015; Pan et al., 2019; Acton et al., 2019). However, such type of stimuli presentation, in which skin is pre-conditioned by removing hair before the experiment, would reduce hair mechanosensory input to the GRPR circuit, probably masking any outcome in response to hair activation.

Concomitant ablation of GRPR with Ptf1a^{EX1} neurons delayed the development of scratching phenotype for more than one day in average. These data indicate that GRPR neurons normally receive direct or indirectly mechanosensory cutaneous information. It has been recently shown that GRPR neurons require a strong excitatory drive from GRP neurons to elicit action potential firing (Pagani et al., 2019). Considering that 90% of body surface in mammals is covered by hairy skin (Djouhri et al., 2016), it is tempting to speculate that mechanosensory input to the circuit is used to maintain GRPR neurons at a high subthreshold level of excitation. Some evidence for this mechanism comes from the observation that GRPR specific activation (Figure 7C and Bardoni et al., 2018) evokes not only scratching behavior but also intense grooming activity (Figure 7D). It remains to be tested, albeit difficult to accomplish, the behavioral response elicited by GRPR activation in the absence of cutaneous mechanosensory information.

Conclusions

Our survival depends on a proper interaction with the outside world. Only a sensory system able to distinguish stimuli originated in the outside world from those originated by the activity of the organism would entail such organism with a good chance to survive. The spinal circuits described here sheds light on how a subtype of inhibitory neurons gates self-generated mechanosensory information during ongoing locomotor activity. Malfunction of this mechanism evolves in a chronic itch syndrome reminiscent of many human pathologies where absence of perceived external stimulus ignites a strong itch-scratch cycle. Despite recent efforts toward the identification of the remaining itch circuit components, many essential questions remain to be solved in order to improve and design new therapies to fight such a debilitating disease as chronic itch.

Materials and Methods

Mouse lines

The mouse lines used in this study were previously described: Ptf1a$^{Cre(ex1)}$ (also known as p48^{Cre}) (Nakhai et al., 2007); Ptf1a$^{Cre(CVW)}$ (Kawaguchi et al., 2002); Tau$^{lsl\text{-}SynaptophysinGFP}$ (Tripodi et al., 2011); Ai9$^{lsl\text{-}tdTomato}$ (B6.Cg-Gt(ROSA)26Sor$^{tm9(CAG\text{-}tdTomato)Hze}$/J) (Madisen et al., 2010); Cdx2^{FlpO} (Britz et al., 2015); Lmx1b^{Cre} (Li et al., 2010); Tau$^{ds\text{-}DTR}$ (Britz et al., 2015); RC::FL-hM3Dq (Sciolino et al., 2016); Ai65D$^{ds\text{-}tdTomato}$ (B6;129S-Gt(ROSA)26Sor$^{tm65.1(CAG\text{-}tdTomato)Hze}$/J) (Madisen et al., 2015); RΦGT (Takatoh et al, 2013); GRPR^{iCre} (Aresh et al., 2017). Animals were kept and used in accordance with regulations from the government of Upper Bavaria. All lines were back-crossed to C57BL/6J mice at least 5 generations.

Monosynaptic rabies virus tracings

Adult mice were anesthesia was induced with isofluorane (2%) and placed in a stereotaxic frame (SR-5M-HT, Narishige) with a heating pad. Anesthesia was maintained throughout the procedures at 1.5% with a nose mask (GM-4, Narishige). The analgesics Metamizol (0.2 mg/g bodyweight, oral) and Carprofen (5mg/kg bodyweight, subcutaneous) were administrated. After incision of the skin and removal of dorsal intervertebral muscles, the vertebral column was fixed with a spinal column clamp (STS-A, Narishige). A laminectomy was performed at the C2 or L1 levels, the dura matter was carefully perforated with a fine needle to expose the spinal cord. 300 nl of virus were injected unilaterally on the dorsal spinal cord 500 µm lateral to the medial artery with a fine glass capillary using a microcontroller. The skin was then closed using a Reflex 7 skin closure system and tissue adhesive (3M Vetbond). Animals were perfused 6 days post-infection. The EnvA G-deleted rabies-GFP (Wickersham et al., 2006) were produced at the Salk Gene Transfer.

Histology

Animals were deeply anesthetized with ketamine/xylazin (100 mg/kg and 16 mg/kg respectively) and transcardially perfused first with phosphate-buffered saline (PBS) and then with 4% paraformaldehyde (PFA) in PBS. Brains and spinal cords were dissected, postfixed at 4°C in 4% PFA overnight, washed in PBS and embedded in 4% agarose. 70- to 100-µm sections were cut with a vibratome (Leica) and sections stored in cryoprotective solution (40% PBS, 30% glycerol, 30% ethylene glycol) at -20°C until use. Embryonic spinal cords were dissected and fixed in 4% PFA in PBS for 2h and processed as described above. DRGs were cryopreserved sequentially in 15% and 30% sucrose in PBS at 4°C, embedded in O.C.T (Fisher Scientific) and cut in a cryostat (Leica). 30 µm sections were mounted on slides, air dried and stored at −80°C.

Immunohistochemistry

For immunofluorescence, vibratome free-floating sections and cryosections were blocked and permeabilized with 5% donkey serum, 0.3% TritonX-100 in PBS for 2 hours at room temperature (RT), following incubation with primary antibodies overnight at 4°C in 0.3% TritonX-100 in PBS. The following primary antibodies were used: goat anti-Pax2 (1:500) (AF3364, R&D Systems), guinea pig anti-Lmx1b (1:10,000) (gift from C. Birchmeier, Max Delbrück Center for Molecular Medicine, Germany), rabbit anti-cFos (1:2000) (sc-52, Santa Cruz), rabbit monoclonal anti-cFos (1:2000) (2250S, Cell signaling), rat anti-mCherry (1:1500) (M11217, Thermo), chicken anti-GFP (1:2000) (GFP-1010, Aves-Labs), chicken anti-βgalactosidase (ab9361, Abcam), anti-NF (1:1000) (NA1211, Affiniti), goat anti-TrkC (1:500) (AF1404, R&D Systems), sheep anti-TH (1:1000) (AB1542, Millipore), guinea pig anti-vGluT2 (1:1000) (AB2251, Millipore), guinea pig anti-vGluT1 (1:1500) (AB5905, Millipore), rabbit anti-DsRed (1:1000) (632496, Clontech), goat anti-CGRP (1:500) (36001, Abcam), rabbit anti-NPY (1:1000) (T-4070.0050, Peninsula Laboratories), goat anti-nNOS (1:1000) (ab1376, Abcam), rabbit anti-vGAT (1:1000) (131002, Synaptic Systems), rabbit anti-ENK (1:1000) (20065, Immunostar), mouse anti-GAD65 (1:50) (GAD6, Developmental Studies Hybridoma Bank, created by the NICHD of the NIH and maintained at The University of Iowa, Department of Biology, Iowa City, IA 52242), rabbit anti-Galanin (1:1000) (T-4334, BMA Biomed), rabbit anti-RFP (1:1000) (600-401-379, Rockland). After three 10-min washes in PBS and sections were incubated with secondary antibodies for 2 h at room temperature in 0.3% TritonX-100 PBS. The following secondary antibodies or counterstains were used: donkey anti-rabbit/mouse/goat/sheep/rat/chicken/guinea pig conjugated to Alexa Fluor 488, Cy3, Alexa Fluor 647 or Cy5 (1:500), Neurotrace 640/660 (1:200) (N-21483, Molecular Probes) or DAPI (1:1000). After three 15-min washes in PBS, sections were mounted in slides and coverslipped with mowiol mounting medium.

Microscopy

Fluorescence z-stack images were acquired with an Olympus FV1000 or Leica SP8 confocal microscope. Images were minimally processed with FiJi/ImageJ software (NIH) or Adobe Photoshop to enhance brightness and contrast. No filters were used to decrease noise. Co-localization analysis quantification was done in single confocal z-sections. Measurements were performed using FiJi/ImageJ software.

For analysis of GFP co-localization with vGAT in presynaptic puncta, 20-60 dorsal horn randomly selected vGlut1/vGAT appositions were marked in ImageJ per hemisection without visualizing the GFP channel. Percentages of vGlut1/vGAT appositions in which the vGAT terminal was also GFP were calculated after revealing the GFP channel. For analysis of vGlut1/vGAT appositions in DTx treated animals, 50 randomly selected vGlut1 terminals were marked in ImageJ per hemisection without visualizing the vGAT channel. Percentages of vGlut1 terminals apposed by vGAT synapses were calculated after revealing the vGAT channel.

Spatial distribution of neurons

The position of interneurons in the spinal cord was recorded manually in FiJi/ImageJ. Cartesian coordinates for each interneuron were determined in the transverse spinal cord plane with respect to the midpoint of the central canal, defined as position (0,0). Custom Python scripts were used to calculate the probability density function and display two-dimensional kernel density estimations for each cell population. Estimates were graphically displayed as shaded or line contour plots, with lines connecting points of equal probability density.

Pharmacological treatments

Ablation was induced by intraperitoneal administration of diphtheria toxin at 50ng/g of body weight (D0564, Sigma-Aldrich) in saline solution. Injection was performed twice with a 72 hours interval (Duan et al., 2014; Bourane et al., 2015; Acton et al., 2019; Pan et al., 2019). GRPR antagonist RC-3095 (Tocris) was dissolved in 0.1% DMSO in saline to 2µg/µl and injected intraperitoneally at 10µg/g of body weight 30 minutes before behavioral evaluation. DREADD activation was induced by intraperitoneal injection of CNO (C0832, Sigma-Aldrich) at 2ng/g of body weight diluted in vehicle (2% DMSO in saline), behavioral tests were performed 30 minutes later.

Behavior assays

Animals were acclimated to the behavioral room and testing apparatus during three consecutive days for at least 30 minutes unless otherwise indicated. Efforts were made to remain blind to the genotype of the tested animals, however given the obvious nature of the phenotype in Ptf1a-ablated animals it was not always possible. Littermates of either sex were used in all tests. Except for the hot plate and rotarod, all the testing apparatuses were custom designed and built from acrylic. Drawings are available upon request.

Home cage video recording (as in Figure 4C, 4D, 4I, …). Animals were single housed at least one week before DTx treatment. Before DT1, animals in their home cages were video recorded with cage lid and food tray removed. A transparent lamina of acrylic was used to prevent animals from getting out. Mice were recorded in pairs for 10 minutes. To evaluate the influence of bedding material in spontaneous scratching behavior, a clean cage without bedding was stacked inside the home cage to preserve as much as possible olfactory cues. The double cage was returned to the rack for 30 minutes and another video recording of 10 minutes was acquired. To evaluate the role of GRPR neurons in Ptf1a-mediated scratching, mice were injected with the GRPR antagonist RC-3095, returned to the double cage and rack for 30 minutes and another video recording of 10 minutes was acquired. Both scratching frequency and grooming time were calculated offline. To evaluate the influence of locomotor activity on scratching behavior (Figure 5J-K), Ptf1a-ablated mice at peak scratching frequency and control littermates were recorded in their home cages 30 minutes after returning them to the cage rack.

Chemical itch. Animals were lightly anesthetized with isofluorane and injected in the back skin at the level of thoracic vertebrae 12. Compound 48/80 (100 ug, Millipore) or chloroquine (200 ug, Millipore) in 50 uL of sterile saline were injected. Animals were video recorded for 30 minutes and the scratching bouts after injection counted.

Hairy skin sensitivity. To evaluate changes in hairy skin sensitivity at different air puff intensities we adapted a previously published system (Orefice et al., 2016). We used a SR-LAB startle response system (SDI-2325-0400, San Diego Instruments) adapted to deliver air puffs (SDI-2325-0368) to the back of the animal. Pressure regulation was achieved through a forward pressure reducing regulator (4136ANNKE, Equilibar). Animals were habituated for 10 minutes to the holding cylinder, noise and light levels the day before testing. Continuous white noise level was set to 90dB to prevent mice from hearing the opening of the valve. The protocol consisted of 5 min acclimatation, followed by 7 trains of 5 air puffs each delivered at pseudorandom interstimulus intervals at increasing preassures from 0.05 PSI to 2.5 PSI.

cFos induction through hair stimulation. To assess the ability of hair movement to induce neuronal activity in the spinal dorsal horn, we adapted a previous protocol designed to stimulate the skin (Duan et al., 2014). We kept mice under light anesthesia (1-1.5% isofluorane) using a head mask. Manipulation of the animal was reduced to the minimum possible to avoid confounding stimulations. The back hairs of the animal were combed with a soft paintbrush (#6) rostrocaudally and caudorostrally from the forelimbs to the hindlimbs for 150 times in 5 minutes. This protocol was applied 3 times with 1 minute intertrials (450 strokes in total during 17 minutes). After stimulation animals were kept under anesthesia for 2 hours, transcardially perfused and processed as previously described for cFos immunostaining.

Dynamic brush. Light touch sensitivity was evaluated with the dynamic light brush test (Bourane et al., 2015). Mice were placed in individual compartments of a testing apparatus with a wire mesh floor. The plantar surface of the hindpaw was lightly stimulated with a soft brush (#6) stroking from heel to toe. Stimulation was repeated 10 times on alternating sides and the percentage of paw withdrawal were calculated.

Von Frey. This test was used to assess sensitivity to static touch and mechanical pain. Mice were placed in individual compartments of a testing apparatus with a wire mesh floor. Calibrated von Frey monofilaments (0.02-2 g) (Aesthesio Precision Tactile Sensory Evaluator) were used to stimulate the medial plantar surface of the hindpaws. Withdrawal, licking or biting following or immediately after the 5 seconds stimulus were considered as a positive response. Paw withdrawal threshold (PWT) were calculated according to (Detloff et al., 2012).

Pinprick. This test was used to evaluate mechanical pain. Mice were placed in individual compartments of a testing apparatus with a wire mesh floor. The plantar surface of the hindpaw stimulated with an Austerlitz insect pin (0.02 mm; Fine Science Tools). Stimulation was repeated 10 times on alternating sides and the percentage of paw withdrawal were calculated.

Dynamic hot plate. Heat sensitivity was evaluated through determination of the thermal withdrawal threshold. Mice were acclimated to the testing apparatus (IITC Life Science) set at 32°C the day before and the testing day for 10 minutes. The assay consisted on 3 trials in which the plate temperature increased from 32°C to 55°C at a rate of 3°C/minute. The ramp was stopped when the animals licked, shooked the hindpaw or jumped.

Cold plantar assay. Cold sensitivity was measured as previously described (Brenner et al., 2012). Mice were placed in individual compartments of a testing apparatus with a 4 mm glass floor. A

pellet of crushed dry ice was positioned in contact with the glass beneath the hindpaw. The stimulus was presented 6 times on alternating sides. Latency to withdrawal was measured.

Acute mechanical itch. We performed two versions of this test, one applying the stimulus to the shaved nape of the neck and another one to the shaved back of the animal according to Bourane et al., 2015. Mice were placed in individual compartments of a testing apparatus with a wire mesh floor and after 30 minutes habituation, received five separate stimuli for ~1 second at random sites on the skin of the target region with a von Frey monofilament of 0.07g. Scratching of the poked site was considered a positive response.

Rotarod. An accelerating rotarod (Ugo Basile) test was used to evaluate gross motor coordination. Mice were trained on 2 consecutive days at a constant speed of 5 rpm for 5 minutes. The training was repeated until each animal stayed in the cylinder without falling down for the whole 5 minutes. The third day the rotarod was programmed to accelerate from 5 to 40 rpm in 5 minutes. Each animal was subject to 3 trials with an intertrial recovery of 15 minutes. Latency to fall, maximum speed and distance walked were registered for each animal.

Open field. Overall locomotor activity and anxiety was evaluated in a custom-made acrylic 40x40x25 cm square arena. Mice were free to explore it for 15 minutes. Mean speed, distance traveled and time spent in the center of the arena (defined as a central 20x20 cm area) was measured with Ethovision XT 11 (Noldus).

Startle reflex/Prepulse inhibition (PPI). PPI testing was performed essentially as a previously described (Orefice et al., 2016; Orefice et al., 2019) with some modifications. The tests were carried out on the same setup used for testing hairy skin sensitivity. Here we evaluated the ability of a tactile pre-stimulus (0.9 PSI, 50 ms) to inhibit startle to a stronger tactile stimulus (3 PSI, 5 ms) (tactile-tactile PPI test) or to a loud acoustic stimulus (120 dB, 20 ms) (tactile-acoustic PPI test) with an interstimulus interval of 250 ms. We sought to investigate whether Ptf1a- or GRPR-ablated animals exhibit specific tactile sensorimotor gating deficits. Animals were habituated for 10 minutes to the holding cylinder, noise and light levels the day before testing. Both PPI test versions were carried out on different days. On testing day, mice were placed inside the ventilated, cylindrical holder on a platform within a soundproof chamber. Protocols were as described (Orefice et al., 2016): acclimation phase with constant white noise (90 dB) for 5 minutes, block I, block II, block III and block IV trials. All stimuli were pseudorandomly spaced between 15 and 45 seconds. Block I consisted of 5 startle stimuli alone (3 PSI 5 ms or 120 dB white noise for tactile-tactile and tactile-acoustic sessions, respectively), to measure the initial startle reflex. Block II consisted of 5 prepulse stimuli alone (0.9 PSI 50 ms), to measure response to the prepulse stimulus alone. Block III incorporated prepulse/pulse, pulse alone and no stimulation trials. Block IV consisted of 5 startle stimuli alone, to measure habituation. Whole body flinch, or startle reflex, was quantified using an accelerometer sensor measuring the amplitude of movement of the animal within the cylindrical holder.

Long-term surveillance of mice in home cages. The plans for the modified cage lid, infrared LED array, camera, lens, raspberry pi and acquisition code are available upon request. We modified the cage lid for adapting a NoIR PiCamera with a modified M12 220° lens (RP-VC1N, Entaniya) to have direct view of the whole inner space of the home cage. The camera was attached to a

Raspberry Pi 3 Model B (Raspberry Pi Foundation) running Raspbian and the picamera python interface was used to control acquisition and saving of the video stream. An acrylic enclosure was custom built to fit around the home cage and fitted with 5 meters of an 850 nm infrared LED strip (Solarox IR1-60-850, LED1.de). Acrylic diffusers were set in place between the LED strip and the cage walls. Mice were habituated for 24 hours to the enclosure after DT2 and recording started. Video recording was stopped when Ptf1a-animals reached peak scratching frequency. FFmpeg was used to convert raw h264 movie streams to compressed video. A neural network was trained on 2000 frames labelled manually with the position and orientation of the mouse to generate an accurate elipse-fit around the mouse (Geuther et al., 2019) and track all the videos. Output of the trained neural network was used to generate the data necessary to input to JAABA (Kabra et al., 2013) and train a behavior classifier to identify frames in which mice engaged in scratching behavior with the hindpaws. The resulting behavior classifier had an accuracy of 88.4% for scratch frames and 78% for non-scratch frames in videos it had never been trained on (ground-truth). This classifier was applied to all the videos for each animal. Scratching time and speed of the animals were computed (Figure S5A-B).

Scratching in a locomotor-restrictive context (Figure 5L-M). To evaluate the influence of locomotion on scratching frequency, Ptf1a-ablated mice at peak scratching frequency and control littermates were recorded in their home cages (see above) and 30 minutes later inside the same holding cylinder used in the startle reflex system. Animals were habituated for 10 minutes the day before testing and recorded for 10 minutes on testing day. Scratching frequency was quantified offline.

Conditioned Place Aversion (CPA). To test for the valence associated with chemogenetic activation of Ptf1a-derived neurons we performed a CPA test as described in (Vrontou et al., 2013). We designed a custom made acrylic 2-chamber arena (each chamber 15x15x30 cm, connected through a 5x5 cm opening that could be closed). Each chamber was designed with a different pattern of alternating black and white stripes (vertical or horizontal) and different patterned floor to help mice to distinguish each chamber during conditioning. On the first day mice were free to explore both chambers for 30 minutes (Pre-Test). Conditioning started the second day, confining the mouse the initially preferred (IP) chamber with CNO treatment for 30 minutes. The third day the mouse was confined to the initially non preferred chamber (INP) after administration of vehicle. The fourth and fifth day the cycle was repeated. On the sixth day, the mouse was allowed to explore freely both chambers and preference was calculated (Post-Test). Percentage of time spent in each chamber was assessed using Ethovision XT 11 software (Noldus).

Chemogenetic induction of itch and grooming. To evaluate itch and grooming induced behaviors by DREADD mediated activation, mice treated with vehicle or CNO in consecutive days were placed in individual compartments of a testing apparatus with a wire mesh floor. A bottom-up view of the animals was video recorded for offline quantification. Scratching bouts and grooming time were calculated for 30 and 10 minutes, respectively, 30 minutes after treatment.

Statistical analysis

No statistical methods were used to predetermine sample sizes. Data presented as bar graphs indicate mean ± SEM (standard error of the mean). Dots in bar graphs and box plots represent individual values per mouse. Statistical analyses were performed in Python and MATLAB using custom scripts. Significance levels are indicated as follows: $^{ns}p > 0.05$; $*p < 0.05$; $**p < 0.01$; $***p < 0.001$; $****p < 0.0001$.

Acknowledgments

We thank the MPI animal facility for support in mouse lines manteinance; Martyn Goulding (Salk Institute), Patricia Jensen (NIEHS), Silvia Arber (Biozentrum–University of Basel, Friedrich Miescher Institute), Jens Siveke (Technischen Universität München), Benjamin Arenkiel (Baylor College of Medicine) and Malin Lagerström (Uppsala Universitet) for mouse lines; Thomas Müller and Carmen Birchmeier (MDC Berlin) for antibodies; Kenneth Klau and Lisa Koletsou for assistance with animal facility work; Daniel del Toro, Hakan Kucukdereli and Amelia Douglass for constructive discussions. This study was supported by the Max-Planck Society and the Deutsche Forschungsgemeinschaft to R.K.

Author contributions

Conceptualization: A.E. and R.K.; Methodology: A.E.; Validation: A.E. and R.K.; Formal Analysis: A.E.; Investigation: A.E.; Resources: A.E.; Data Curation: A.E.; Writing–Original Draft: A.E. and R.K.; Writing–Review and Editing: A.E. and R.K.; Visualization: A.E.; Supervision: R.K.; Funding Acquisition: R.K.

Declaration of interests

The authors declare no competing interests.

Figure 1

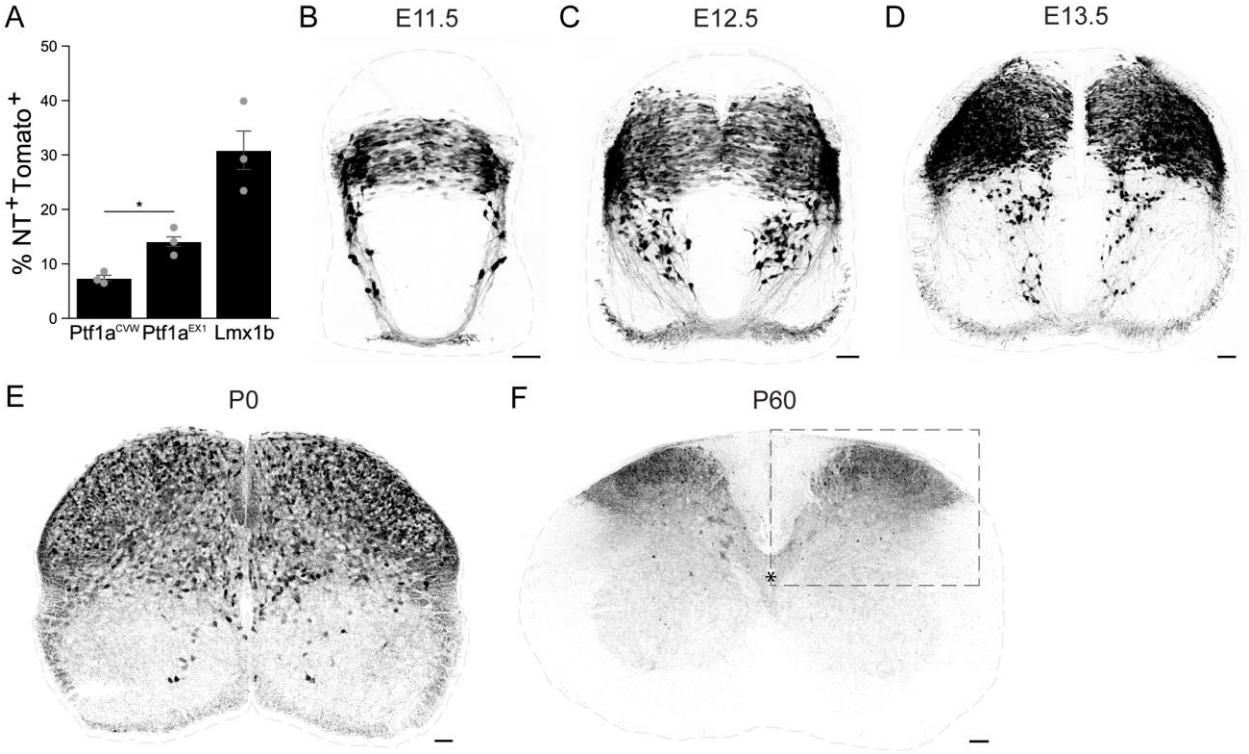

Figure 1. Characterization of Ptf1a^{Cre} mouse lines and ontogenesis of adult Ptf1a-derived neurons in the spinal cord.

A. Quantification of percentage of neurons (NeuroTrace^{+}) in dorsal hemisection of the adult (P60) spinal cord that derive from Ptf1a^{CVW} (7.38±0.64%, n=3 mice), Ptf1a^{EX1} (14±1.5%, n=3 mice) and Lmx1b^{Cre} (31±5%, n=3 mice). Bars represent mean ± SEM. Two-sided Student's unpaired t test, (st=-4.18, *p=0.014).

B-E. Developmental course of Ptf1a^{EX1} spinal neurons in a Tomato reporter mouse line. Notice migration of cells ventrally during early neurogenesis. Scale bar: 50 µm.

F. Distribution of Ptf1a^{EX1};Tomato neurons in the adult spinal cord. Notice almost complete absence of neurons ventral to the central canal (asterisk). Scale bar: 100 µm.

See also Figure S1.

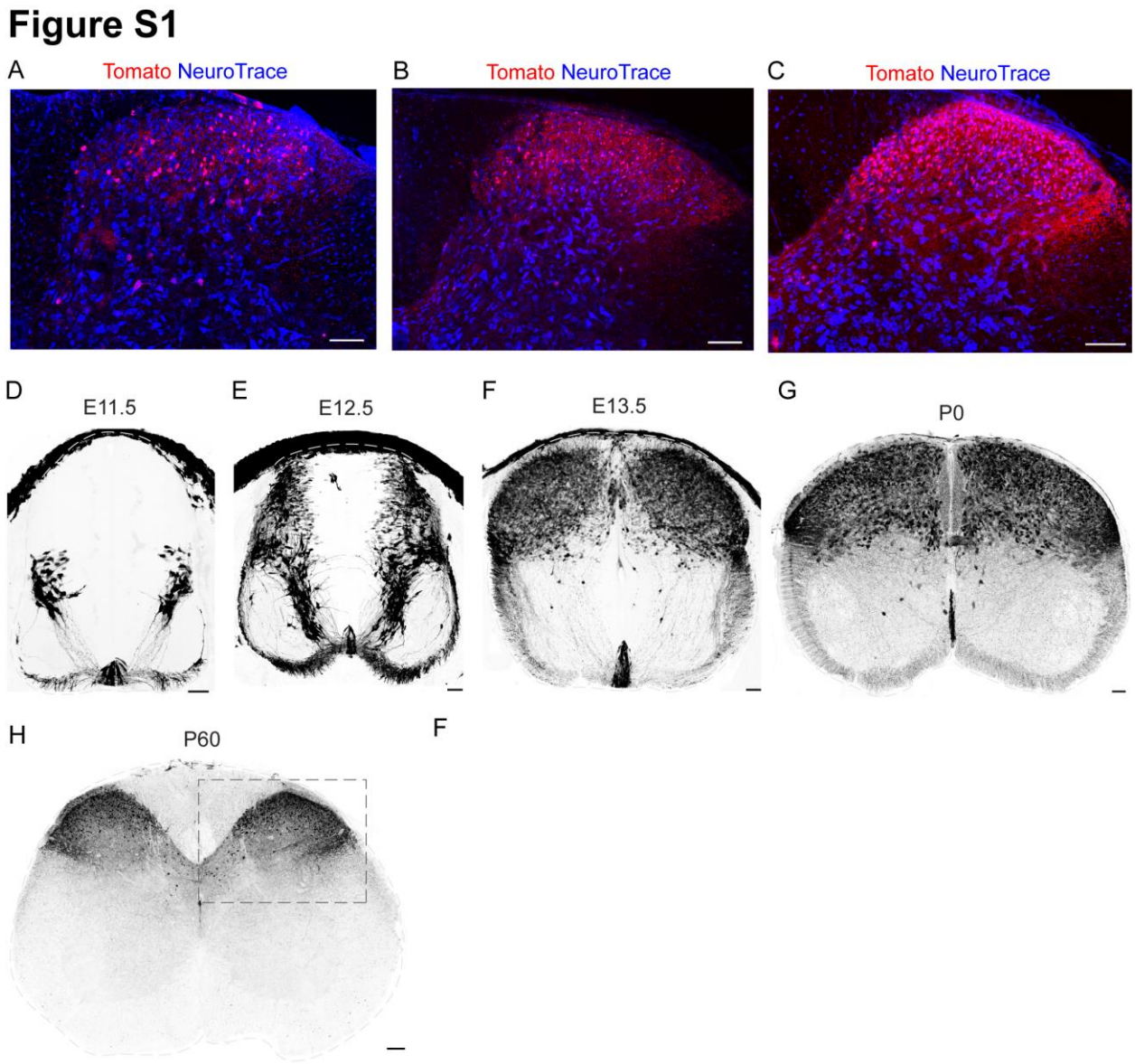

Figure S1. Ontogenesis of adult Lmx1b-derived neurons in the spinal cord (related to Figure 1).

A. High magnification view of the dorsal horn region of adult Ptf1a^{CVW};Tomato in Fig.1 F inset used for quantification. Co-staining for Tomato and NeuroTrace to label neurons. Scale bar: 100 µm.

B. High magnification view of the dorsal horn region of adult Ptf1a^{EX1};Tomato in Fig.1 F inset used for quantification. Co-staining for Tomato and NeuroTrace to label neurons. Scale bar: 100 µm.

C. High magnification view of the dorsal horn region of adult Lmx1b^{Cre};Tomato in H inset used for quantification. Co-staining for Tomato and NeuroTrace to label neurons. Scale bar: 100 µm.

D-G. Developmental course of Lmx1b^{Cre} spinal neurons in a Tomato reporter mouse line. Migration of cells ventrally during early neurogenesis also occurs in this population. Scale bar: 50 µm.

H. Distribution of Lmx1b^{Cre};Tomato neurons in the adult spinal cord. Early ventrally migrating neurons have disappeared at this stage. Scale bar: 100 µm.

Figure 2

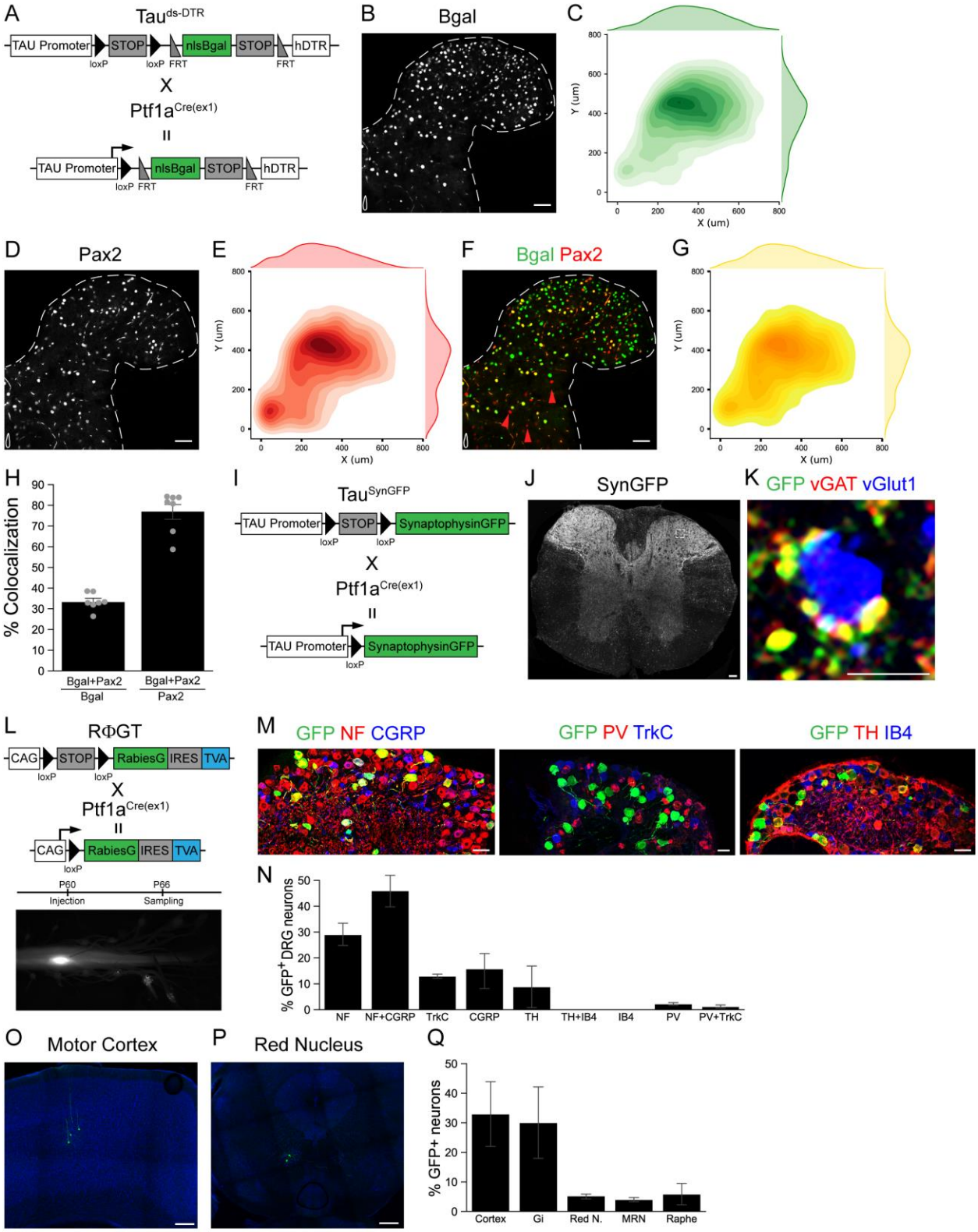
A
Tau^ds-DTR
TAU Promoter
STOP
nlsBgal
STOP
hDTR
loxP
loxP FRT
FRT
X
Ptf1a^Cre(ex1)
TAU Promoter
nlsBgal
STOP
hDTR
loxP FRT
FRT
B
Bgal
C
Y (um)
X (um)
D
Pax2
E
Y (um)
X (um)
F
Bgal Pax2
G
Y (um)
X (um)
H
% Colocalization
Bgal+Pax2
Bgal
Bgal+Pax2
Pax2
I
Tau^SynGFP
TAU Promoter
STOP
SynaptophysinGFP
loxP
loxP
X
Ptf1a^Cre(ex1)
TAU Promoter
SynaptophysinGFP
loxP
J
SynGFP
K
GFP vGAT vGlut1
L
RΦGT
CAG
STOP
RabiesG
IRES
TVA
loxP
loxP
X
Ptf1a^Cre(ex1)
CAG
RabiesG
IRES
TVA
loxP
P60
Injection
P66
Sampling
M
GFP NF CGRP
GFP PV TrkC
GFP TH IB4
N
% GFP+ DRG neurons
NF
NF+CGRP
TrkC
CGRP
TH
TH+IB4
IB4
PV
PV+TrkC
O
Motor Cortex
P
Red Nucleus
Q
% GFP+ neurons
Cortex
Gi
Red N.
MRN
Raphe

Figure 2. Input-output of Ptf1a-derived neurons in the adult spinal cord.

A. Scheme representing the $Tau^{ds\text{-}DTR}$ mouse line used for diphtheria toxin mediated ablation. β-galactosidase expression can be used to track Cre^+ neurons.

B. β-galactosidase immunofluorescence of $Ptf1a^{EX1}$ neurons in the dorsal spinal cord of adult thoracic dorsal horn section. Scale bar: 50 µm.

C. Kernel density estimate plot of the distribution of β-galactosidase$^+$ neurons. 88% of β-gal$^+$ neurons are located 200 µm from the central canal. n = 7 animals, 8472 neurons.

D. Pax2 immunofluorescence channel from same section in C. Scale bar: 50 µm.

E. Kernel density estimate plot of the distribution of Pax2$^+$ neurons. 75% of Pax2$^+$ neurons are located 200 µm from the central canal. n = 7 animals, 3680 neurons.

F. β-gal and Pax2 co-localization in the adult dorsal spinal cord. Red arrows point to Pax2$^+$β-gal$^-$ neurons. Scale bar: 50 µm.

G. Kernel density estimate plot of the distribution of Pax2$^+$β-gal$^+$ neurons. n = 7 animals, 2805 neurons.

H. Quantification of co-localization Pax2 and β-gal in dorsal hemisection of the spinal cord. Pax2$^+$β-gal$^+$ double positive neurons represent 33.5±1.5% of β-gal$^+$ and 77.2±4% of Pax2$^+$. Bars represent mean±SEM. n = 7 animals.

I. Scheme representing the $Tau^{lslSynGFP}$ mouse line used for labelling of presynaptic terminals.

J. Overview of GFP immunofluorescence in an adult thoracic section of spinal cord from $Ptf1a^{EX1}$;SynGFP mouse. Scale bar: 50 µm.

K. High magnification of inset in J showing a sensory terminal expressing vGlut1 (blue) receiving presynaptic inhibitory (vGAT$^+$, red) contacts derived from $Ptf1a^{EX1}$ neurons (green). Scale bar: 2.5 µm.

L. Scheme representing the RΦGT mouse line used for transsynaptic tracing with envelope-A modified rabies virus. Cre recombination leads to the expression of rabies glycoprotein and TVA (upper panel). Rabies virus injection was performed in the spinal cord of adult animals, 6 days later spinal cords, DRGs and brains were processed for immunofluorescence (lower panel).

M. Representative image of dorsal root ganglion showing GFP$^+$ neurons labeled by transsynaptic tracing from Ptf1a-derived neurons. Neurofilament (NF), Calcitonin gene-related peptide (CGRP), Parvalbumin (PV), Tropomyosin receptor kinase C (TrkC), Tyrosine hydroxylase (TH), and Isolectin GS-IB_4 (IB4) immunofluorescence. Scale bar: 50 µm.

N. Quantification of GFP co-localization with sensory neurons markers expressed as percentage of the total of GFP$^+$ neurons. Bars represent mean ± SEM. n = 3 animals per marker combination.

O. Representative image of GFP+ cortical neurons labelled by transsynaptic tracing from Ptf1a-derived neurons in the spinal cord. Scale bar: 200 µm.

P. Representative image of GFP+ red nucleus neurons labelled by transsynaptic tracing from Ptf1a-derived neurons in the spinal cord. Scale bar: 200 µm.

Q. Quantification of supraspinal input regions to Ptf1a-derived neurons of the spinal cord expressed as percentage of the total of GFP^+ neurons found in the brain. Bars represent mean ± SEM. n = 5 animals.

See also Figure S2.

Figure S2

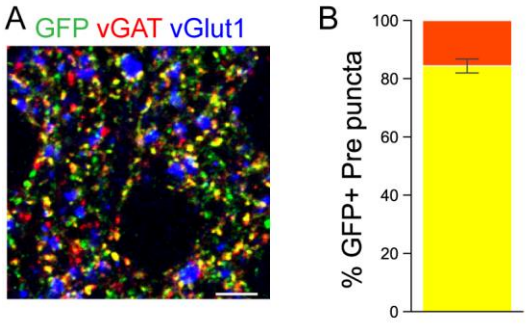

Figure S2. Ptf1a-derived neurons establish presynaptic contacts with mechanosensory terminals in the dorsal horn (related to Figure 2).

A. Representative image of dorsal spinal cord at high magnification showing sensory terminals expressing vGlut1 (blue) receiving presynaptic inhibitory (vGAT^{+}, red) contacts. A high proportion are also GFP (green) derived from Ptf1a^{EX1} neurons. Scale bar: 5 µm.

B. Quantification of proportion vGAT^{+} inhibitory terminals presynaptic to vGlut1 sensory terminals that derive from Ptf1a^{EX1} neurons (84.36±2.66%). Bar represent mean±SEM. n=3 mice.

Figure 3

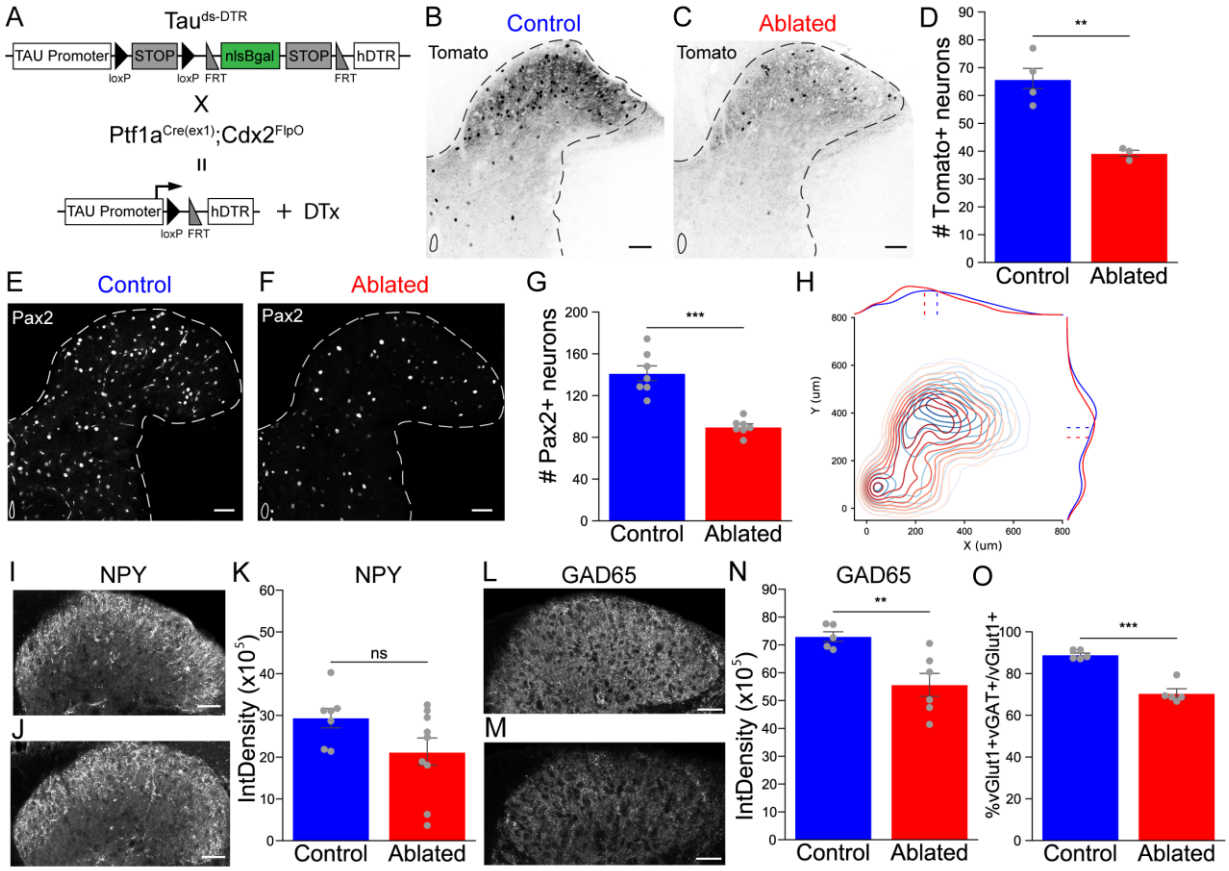

Figure 3. Characterization of diphtheria toxin-mediated ablation of Ptf1a-derived spinal neurons.

A. Scheme representing Cre and FlpO mediated dual recombination of Tau$^{ds\text{-}DTR}$ mouse line used to selectively ablate Ptf1a neurons in the spinal cord. Cells expressing both Cre and FlpO recombinases express the human diphtheria toxin receptor (hDTR) which yields the cell sensitive to diphtheria toxin.

B-C. Representative images of adult thoracic spinal cord hemisection showing Ptf1a-derived neurons expressing Tomato before (B) and one week after (C) diphtheria toxin delivery. Scale bar: 50 µm.

D. Quantification of the number of Tomato^{+} neurons in dorsal hemisection of the spinal cord in control (65.8±4.5 cells) and ablated (39±1 cells) animals. Bars represent mean ± SEM. n = 4 animals per genotype. Two-sided Student's unpaired t test, (st=4.87, **p=0.0045).

E-F. Representative images of Pax2 immunofluorescence in control (E) and Ptf1a-ablated (F) spinal cord dorsal hemisections. Scale bar: 50 µm.

G. Quantification of the number of Pax2$^+$ neurons in dorsal hemisection of the spinal cord in control (141.36±7.75 cells) and Ptf1a-ablated (89.96±2.92 cells) animals. Bars represent mean ± SEM. n = 7 animals per genotype. Two-sided Welch's unpaired t test, (st=6.20, ***p=0.0003).

H. Kernel density estimate plot of the distribution of Pax2$^+$ neurons in control (blue) and Ptf1a-ablated (red) spinal cords. Pax2$^+$ neurons in Ptf1a-ablated animals occupy a more medial (median: 237.8 µm vs 289 µm) and ventral (median: 297.7 µm vs 338.4 µm) position with respect to control animals. n = 7 animals each group, control: 3680 neurons, ablated: 2451 neurons.

I-J. Representative images of NPY immunofluorescence in control (L) and Ptf1a-ablated (M) spinal cord dorsal horns. Scale bar: 50 µm.

K. Quantification of Neuropeptide Y immunofluorescence integrated density in the dorsal horn of control ($2.94x10^6$±$2.44x10^5$ A.U.) and Ptf1a-ablated neurons ($2.12x10^6$±$3.48x10^5$ A.U.). Bars represent mean ± SEM. n = 7 animals per genotype. Two-sided Student's unpaired t test, (st= 1.818, ^{ns}p= 0.0904).

L-M. Representative images of GAD65 immunofluorescence in control (I) and Ptf1a-ablated (J) spinal cord dorsal horns. Scale bar: 50 µm.

N. Quantification of GAD65 immunofluorescence integrated density in the dorsal horn of control ($7.3x10^6$±$1.9x10^5$ A.U.) and Ptf1a-ablated neurons ($5.5x10^6$±$4.5x10^5$ A.U.). Bars represent mean ± SEM. n = 7 animals per genotype. Two-sided Student's unpaired t test, (st=3.278, **p= 0.0095).

O. Quantification of the percentage of vGlut1+ sensory terminals apposed by vGAT+ inhibitory synapses in the dorsal horn of control (blue, 88.99±0.96%) and Ptf1a-ablated animals (red, 70.53±2.44%). Bars represent mean ± SEM. n = 5 animals per genotype. Two-sided Student's unpaired t test, (st=7.5, ***p=0.00044).

See also Figure S3.

Figure S3

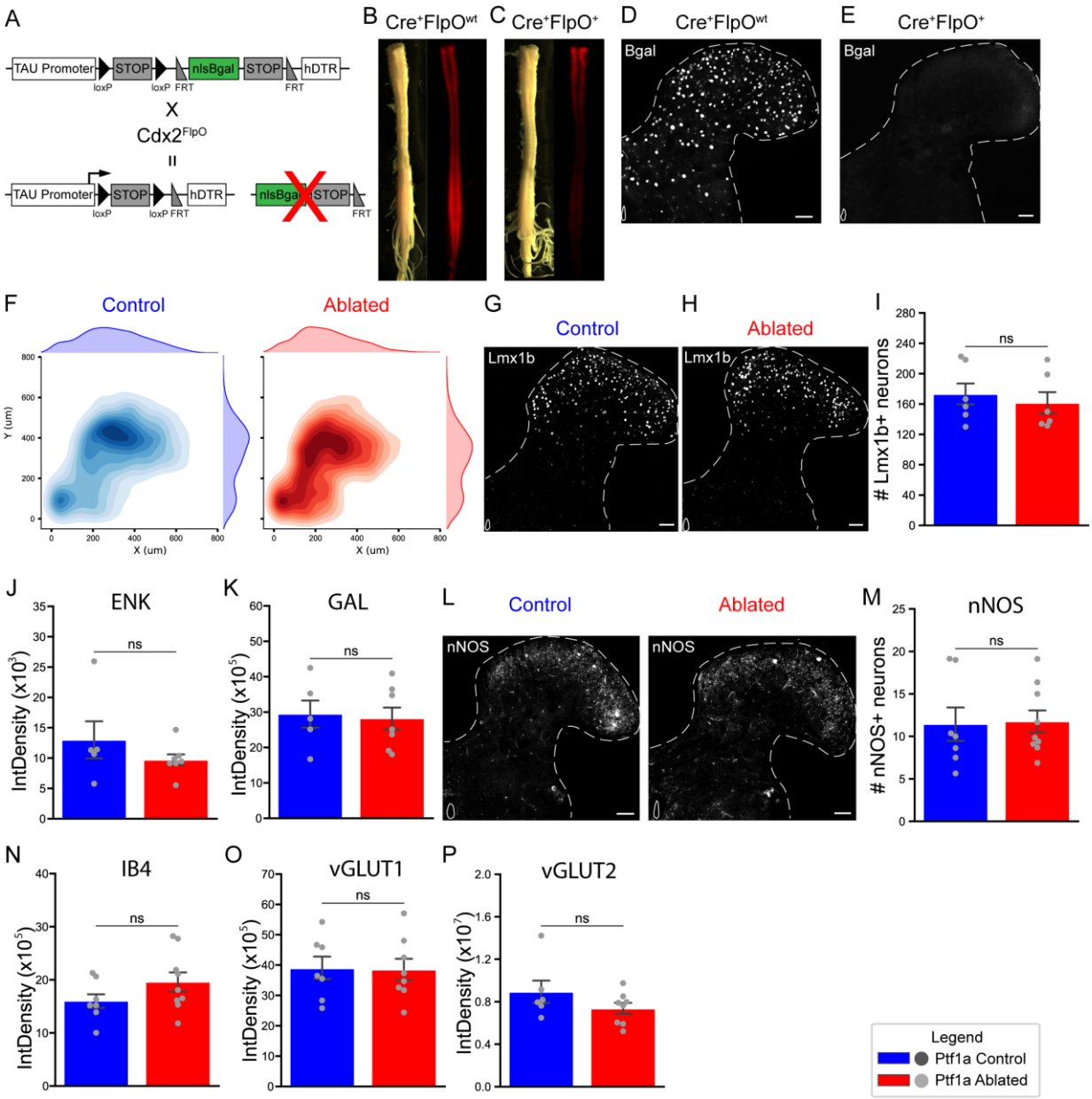

Figure S3. Further characterization of diphtheria toxin-mediated ablation of Ptf1a-derived spinal neurons. (related to Figure 3).

A. Scheme representing FlpO mediated recombination of Tau$^{ds\text{-}DTR}$ mouse line used to direct spatial selective expression of hDTR in the spinal cord. Cells expressing FlpO recombinase lose expression of the marker β-galactosidase, which allows to assess the co-expression of Cre and FlpO in the same cell.

B-C. Full view of dissected spinal cords from animals positive only for Cre (B) and animals expressing both Cre and FlpO (C) together with Ai9^{lsltdTomato} reporter allele. The Cdx2^{FlpO} mouse

line drives expression from midcervical levels to the caudal end of the spinal cord as it can be observed in C by the loss of Tomato fluorescence (in each panel: left, visible light; right, tomato fluorescence).

D-E. Representative images of β-galactosidase immunofluorescence in spinal cord section from animal expressing Cre (D) and animal expressing both Cre and FlpO (D). Loss of β-galactosidase signal in all of the Ptf1a-derived cells indicate expression of FlpO in all Cre^+ neurons. Scale bar: 50 µm.

F. Individual kernel density estimate plots of the distribution of $Pax2^+$ neurons in control (blue) and Ptf1a-ablated (red) spinal cords shown in Figure 3H. n = 7 animals each group, control: 3680 neurons, ablated: 2451 neurons.

G-H. Representative images of Lmx1b immunofluorescence in control (G) and Ptf1a-ablated (H) spinal cord dorsal hemisections. Scale bar: 50 µm.

I. Quantification of the number of $Lmx1b^+$ neurons in dorsal hemisections of the spinal cord in control (173.33±15.72 cells) and Ptf1a-ablated (161.73±15.30 cells) animals. Bars represent mean ± SEM. n = 6/7 animals per genotype. Two-sided Student's unpaired t test, (st= 0.5287, ^{ns}p= 0.6085).

J. Quantification of Enkephalin immunofluorescence integrated density in the dorsal horn of control ($1.3x10^4$±$3.4x10^3$ A.U.) and Ptf1a-ablated neurons ($9.7x10^3$±$1.02x10^3$ A.U.). Bars represent mean ± SEM. n = 5/7 animals per genotype. Two-sided Welch's unpaired t test, (st= 0.927, ^{ns}p= 0.3988).

K. Quantification of Galanin immunofluorescence integrated density in the dorsal horn of control ($2.95x10^6$±$4.4x10^5$ A.U.) and Ptf1a-ablated neurons ($2.82x10^6$±$3.4x10^5$ A.U.). Bars represent mean ± SEM. n = 5/7 animals per genotype. Two-sided Student's unpaired t test, (st= 0.2287, ^{ns}p= 0.8237).

L. Representative images of nNOS immunofluorescence in control (O) and Ptf1a-ablated (P) spinal cord dorsal hemisections. Scale bar: 50 µm.

M. Quantification of the number of $nNOS^+$ neurons in dorsal hemisections of the spinal cord in control (11.46±2.05 cells) and Ptf1a-ablated (11.78±1.37 cells) animals. Bars represent mean ± SEM. n = 7 animals per genotype. Two-sided Student's unpaired t test, (st= -0.1349, ^{ns}p= 0.8946).

N. Quantification of IB4 immunofluorescence integrated density in the dorsal horn of control ($1.6x10^6$±$1.47x10^5$ A.U.) and Ptf1a-ablated neurons ($1.96x10^6$±$1.87x10^5$ A.U.). Bars represent mean ± SEM. n = 7 animals per genotype. Two-sided Student's unpaired t test, (st= -1.4297, ^{ns}p= 0.1747).

O. Quantification of vGlut1 immunofluorescence integrated density in the dorsal horn of control ($3.89x10^6$±$3.91x10^5$ A.U.) and Ptf1a-ablated neurons ($3.85x10^6$±$3.65x10^5$ A.U.). Bars represent mean ± SEM. n = 7 animals per genotype. Two-sided Student's unpaired t test, (st= 0.084, ^{ns}p=0.934).

P. Quantification of vGlut2 immunofluorescence integrated density in the dorsal horn of control ($10^6 \pm x10^5$ A.U.) and Ptf1a-ablated neurons ($x10^6 \pm x10^5$ A.U.). Bars represent mean ± SEM. n = 7 animals per genotype. Two-sided Mann Whitney u test, (st= 32.0, $^{ns}p=0.3329$).

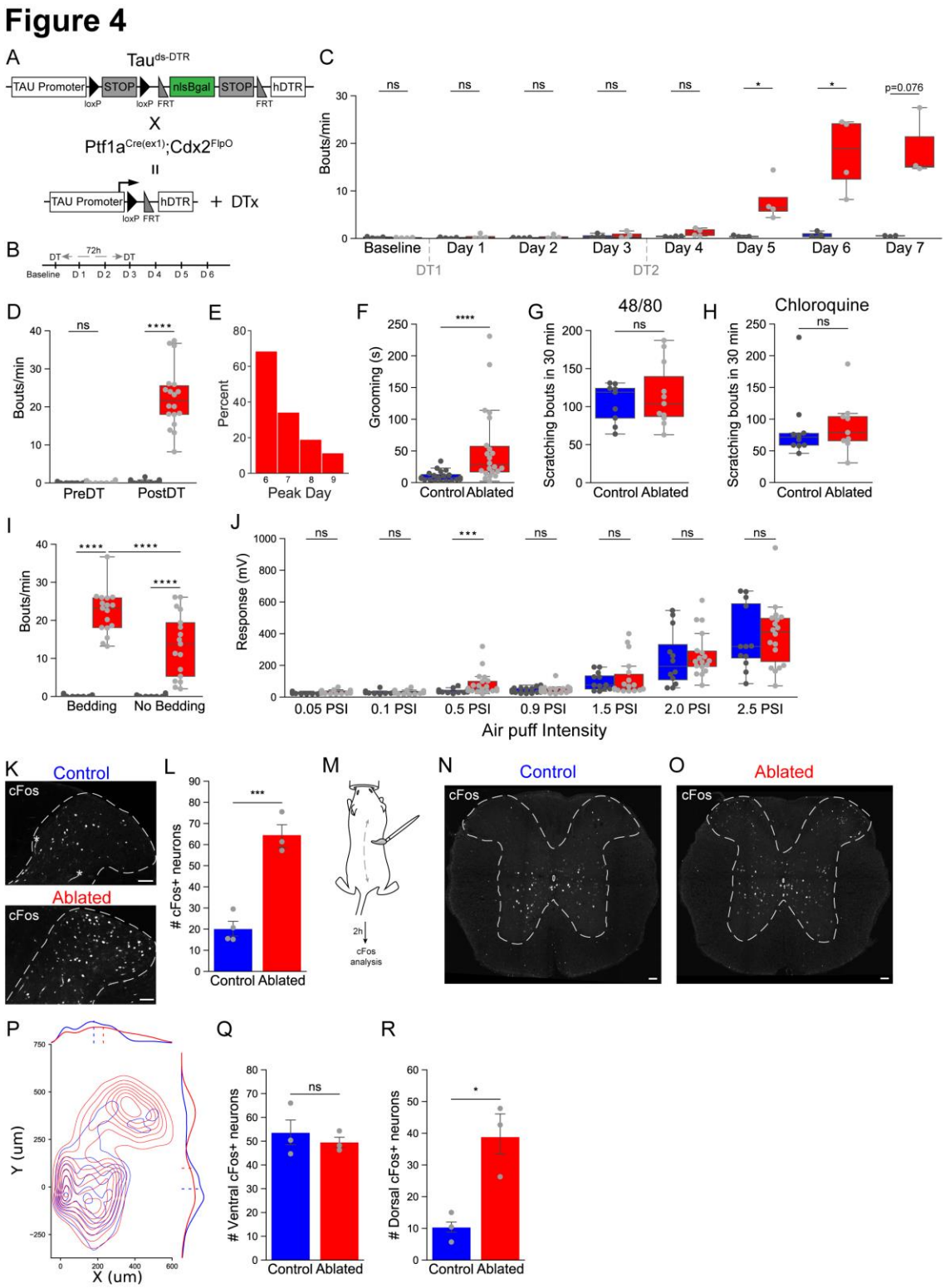

Figure 4. Loss of Ptf1a-derived spinal neurons results in fur movement-dependent itch.

A-B. Schematic representation of genetic crosses (A) and testing (B) of animals. Each mouse was single-housed, injected twice with diphtheria toxin and video recorded in their home cage for 8 days. See Material and Methods for details.

C. Time course development of the scratching phenotype in the first cohort of control (blue) and Ptf1a-ablated (red) animals. DT1 and DT2 depicts the timing of diphtheria toxin delivery. n = 4 animals per genotype and timepoint. Day 7 only includes 3 animals due to the sacrifice of one animal according to ethical considerations. Baseline: Control 0.2±0.09 vs Ablated 0.15±0.03 bouts/min, Day 1: Control 0.15±0.06 vs Ablated 0.37±0.24 bouts/min, Day 2: 0.15±0.03 vs Ablated 0.3±0.2 bouts/min, Day 3: Control 0.47±0.21 vs Ablated 0.62±0.36 bouts/min, Day 4: Control 0.4±0.07 vs Ablated 1.27±0.41 bouts/min, Day 5: Control 0.4±0.12 vs Ablated 7.92±2.21 bouts/min, Day 6: 0.75±0.31 vs Ablated 17.65±3.98 bouts/min, Day 7: Control 0.53±0.06 vs Ablated 19.16±4.2 bouts/min. Two-sided Mann Whitney's unpaired u test, $^{ns}p>0.05$, $*p<0.05$.

D. Quantification of scratching frequency in control (blue) and Ptf1a-ablated (red) animals in their home cages, before and after DT treatment. n =16/18 animals per genotype. Control PreDT: 0.187±0.044 bouts/minute, Control PostDT: 0.337±0.111 bouts/minute, Ablated PreDT: 0.166±0.050, Ablated PostDT: 22.40±1.918 bouts/minute. Two-sided Mann Whitney's unpaired u test: PreDT (st= 159.5, $^{ns}p= 0.5944$), PostDT (st=0, ****$p= 6.79x10^{-7}$).

E. Histogram representing percentage of Ptf1a-ablated animals expressing maximum scratching frequency in relation to timing after DT1: Day 6 68.57%, Day 7 34.28%, Day 8 19.04%, Day 9 11.4%. n = 35 animals.

F. Quantification of time spent grooming for control (blue) and Ptf1a-ablated (red) animals in their home cages after DT treatment. n =20/22 animals per group. Control: 10.02±1.84 seconds, Ablated: 53.84±12.81 seconds. Two-sided Mann Whitney's unpaired u test, (st=65.0, ****$p=9.98 x10^{-5}$).

G. Quantification of scratching bouts in control (blue) and Ptf1a-ablated (red) animals after injection of compound 48/80 into the back 5 days after DT1. n = 9/11 animals per group. Control: 105.11±8.62 bouts/minute, Ablated: 115.27±12.64 bouts/minute. Two-sided Student's unpaired t test, (st= -0.633, $^{ns}p=0.534$).

H. Quantification of scratching bouts in control (blue) and Ptf1a-ablated (red) animals after injection of chloroquine into the back 5 days after DT1. Control: 85.5±16.78 bouts/minute, n=10 mice, Ablated: 89.77±14.66 bouts/minute, n=9 mice. Two-sided Mann Whitney's unpaired u test, (st=35.0, $^{ns}p=0.4377$).

I. Quantification of scratching frequency in control (blue) and Ptf1a-ablated (red) animals in their home cages 30 minutes after removal of bedding material. n = 14/17 animals per group. Control Bedding: 0.17±0.06 bouts/minute, Control No Bedding: 0.17± 0.07 bouts/minute, Ablated Bedding: 22.16±1.4, Ablated No Bedding: 13.43± 2.04 bouts/minute. Two-sided Mann Whitney unpaired u test, Bedding (st= 0, ****$p= 2.31 x10^{-6}$), No Bedding (st=0, ****$p= 2.207 x10^{-6}$). Two-sided Student's paired t test, Ablated (st=5.77, ****$p=2.84 x10^{-5}$).

J. Quantification of the activity response elicited by air puffs of increasing intensity directed towards the back of control (blue) and Ptf1a-ablated (red) animals 5 days after DT1. n = 12-21 animals per group and timepoint. Two-sided Mann Whitney's unpaired u test, ***$p < 0.001$.

K. Representative images of cFos immunofluorescence in control (upper) and Ptf1a-ablated (lower) spinal cord dorsal hemisections after DT treatment. Asterisks: example of non-specifically labelled blood vessels. Scale bar: 50 µm.

L. Quantification of the number of $cFos^+$ neurons in dorsal hemisections of the spinal cord in control (20.2±3.34 cells, n=4 mice) and Ptf1a-ablated (64.66±5.55 cells, n=3 mice) animals. Bars represent mean ± SEM. Two-sided Student's unpaired t test, (st=-7.289, ***p=0.00076).

M. Schematic representation of cFos induction through fur stimulation.

N-O. Representative images of cFos immunofluorescence in control (N) and Ptf1a-ablated (O) spinal cord dorsal sections after DT treatment and fur stimulation protocol. Notice how the number of cFos neurons changes in the dorsal horns. Scale bar: 50 µm.

P. Kernel density estimate plot of the distribution of $cFos^+$ neurons in control (blue) and Ptf1a-ablated (red) spinal cords after back hair stimulation. Ptf1a-ablated animals show an increased number of $cFos^+$ neurons specifically in the dorsal horns compared to control animals. Control: 6150 neurons, n=3 mice, Ablated: 7914 neurons, n=3 mice.

Q. Quantification of the number of $cFos^+$ neurons in ventral spinal cord from control and Ptf1a-ablated animals after fur stimulation protocol. Bars represent mean ± SEM of the number of ventral $cFos^+$ neurons per hemisection. Control (53.7±6.4 cells, n=3 mice), Ablated (49.6±2.43 cells, n=3 mice). Two-sided Student's unpaired t test, (st=0.60, $^{ns}p=0.58$).

R. Quantification of the number of $cFos^+$ neurons in dorsal spinal cord from control and Ptf1a-ablated animals after fur stimulation protocol. Bars represent mean ± SEM of the number of dorsal $cFos^+$ neurons per hemisection. Control (10.4±2.7 cells, n=3 mice), Ablated (38.9±6.5 cells, n=3 mice). Two-sided Student's unpaired t test, (st=-4.056, *p=0.015).

See also Figure S4.

Figure S4

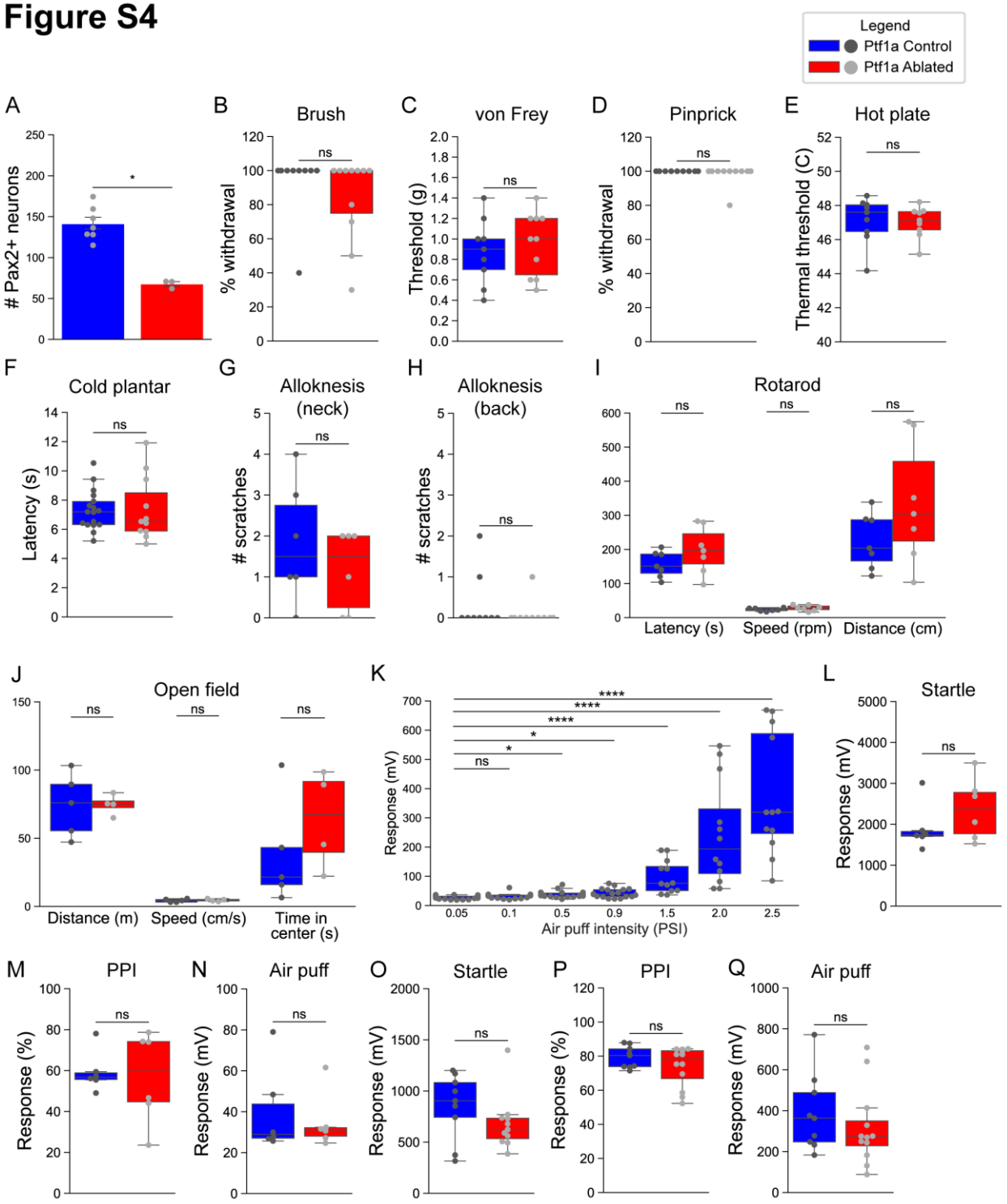

Figure S4. Further behavioral testing Ptf1a-ablated animals (related to Figure 4).

A. Quantification of the number of Pax2⁺ neurons in dorsal hemisections of the spinal cord in control (141.36±7.75 cells, n=7 mice) and Ptf1a-ablated (67.75±2.87 cells, n=3 mice) animals 5 days after DT1. Bars represent mean ± SEM. Two-sided Mann Whitney's unpaired u test, (st= 21.0, *p= 0.022).

B. No differences in dynamic brush test between control (blue, 93.33±6.66%, n=9 mice) and Ptf1a-ablated (red, 84.54±7.43%, n=11 mice) animals 5 days after DT1. Two-sided Mann Whitney's unpaired u test, (st= 61.0, ^{ns}p= 0.272).

C. No differences in von Frey test between control (blue, 0.87±0.1, n=9 mice) and Ptf1a-ablated (red, 0.95±0.1, n=10 mice) animals 5 days after DT1. Two-sided Student's unpaired t test, (st= -0.499, ^{ns}p= 0.623).

D. No differences in pinprick test between control (blue, 100±0%, n=9 mice) and Ptf1a-ablated (red, 98.18±1.81%, n=11 mice) animals 5 days after DT1. Two-sided Mann Whitney's unpaired u test, (st= 54.0, ^{ns}p= 0.421).

E. No differences in hot plate test between control (blue, 47.13±0.45°C, n=9 mice) and Ptf1a-ablated (red, 47.01±0.30°C, n=9 mice) animals 5 days after DT1. Two-sided Student's unpaired t test, (st=0.216, ^{ns}p=0.831).

F. No differences in cold plantar test between control (blue, 7.32±0.33s, n=17 mice) and Ptf1a-ablated (red, 7.36±0.66s, n=11 mice) animals 5 days after DT1. Two-sided Student's unpaired t test, (st= -0.07, ^{ns}p= 0.944).

G. No differences in alloknesis test in shaved neck between control (blue, 1.83±0.6 scratches, n=6 mice) and Ptf1a-ablated (red, 1.16±0.4 scratches, n=6 mice) animals 5 days after DT1. Two-sided Mann Whitney's unpaired u test, (st= 22.5 , ^{ns}p= 0.508).

H. No differences in alloknesis test in back between control (blue, 0.33±0.23 scratches, n=9 mice) and Ptf1a-ablated (red, 0.1±0.09 scratches, n=10 mice) animals 5 days after DT1. Two-sided Mann Whitney's unpaired u test, (st= 51.0, ^{ns}p= 0.44).

I. No differences in rotarod test between control (blue, latency: 156.47±14.38s, speed: 23.66±1.69 rpm, distance: 224.71±30.68 cm, n=7 mice) and Ptf1a-ablated (red, latency: 197.71±25.96s, speed: 28.24±3.06 rpm, distance: 335.55±67.65 cm, n=7 mice) animals 5 days after DT1. Two-sided Student's unpaired t test, Latency: (st= -1.389, ^{ns}p= 0.1899), Speed: (st=-1.305, ^{ns}p=0.216), Distance: (st=-1.49, p=0.161).

J. No differences in open field test between control (blue, distance: 74.32±10.4 m, speed: 4.3±0.52 cm/s, time in center: 38.18±17.43s, n=5 mice) and Ptf1a-ablated (red, distance: 74.65±3.77 m, speed: 4.64±0.45 cm/s, time in center: 63.92±18.1s, n=4 mice) animals 5 days after DT1. Two-sided Student's unpaired t test, Distance: (st= -0.027, ^{ns}p= 0.979), Speed: (st= -0.482, ^{ns}p= 0.645), Time in center: (st= -1.015, ^{ns}p= 0.344).

K. Evaluation of the response of control animals to increasing intensities of air puffs directed to the back hairy skin: 0.05 PSI: 27.25±1.46 mV, 0.1 PSI: 32.41±2.2 mV, 0.5 PSI: 37.7±2.8 mV, 0.9 PSI: 42.03±3.73 mV, 1.5 PSI: 98.52±16.22 mV, 2.0 PSI: 243.83±51.31 mV, 2.5 PSI: 372.8±59.53 mV. n=12-18 animals per intensity. One-way Kruskal-Wallis test followed by post hoc Fisher's least significance difference comparison: ^{ns}p>0.05, *p<0.05, ****p<0.0001.

L-N. No differences in tactile-acoustic startle response test between control (blue, startle: 1905.83±230.21 mV, PPI: 59.25±4.02%, prepulse: 39.6±8.6 mV, n=6 mice) and Ptf1a-ablated (red, startle: 2374±309.5 mV, PPI: 56.88±9%, prepulse: 34.67±5.5 mV, n=6 mice) animals 5 days

after DT1. Two-sided Mann Whitney's unpaired u test, Startle: (st= 13.0, ^{ns}p= 0.4711), Prepulse: (st=17.0, ^{ns}p=0.936). Two-sided Student's unpaired t test, PPI: (st= 0.239, ^{ns}p= 0.815).

O-Q. No differences in tactile-tactile startle response test between control (blue, startle: 849±107.25 mV, PPI: 79.4±2.11%, prepulse: 387.64±62.56 mV, n=9 mice) and Ptf1a-ablated (red, startle: 679.3±80.2 mV, PPI: 73.67±3.42%, prepulse: 317.23±54.25 mV, n=12 mice) animals 5 days after DT1. Two-sided Mann Whitney's unpaired u test, Startle: (st= 69.0, ^{ns}p= 0.148), PPI: (st= 65.0, ^{ns}p= 0.455). Two-sided Student's unpaired t test, Prepulse: (st= 0.85, ^{ns}p= 0.406).

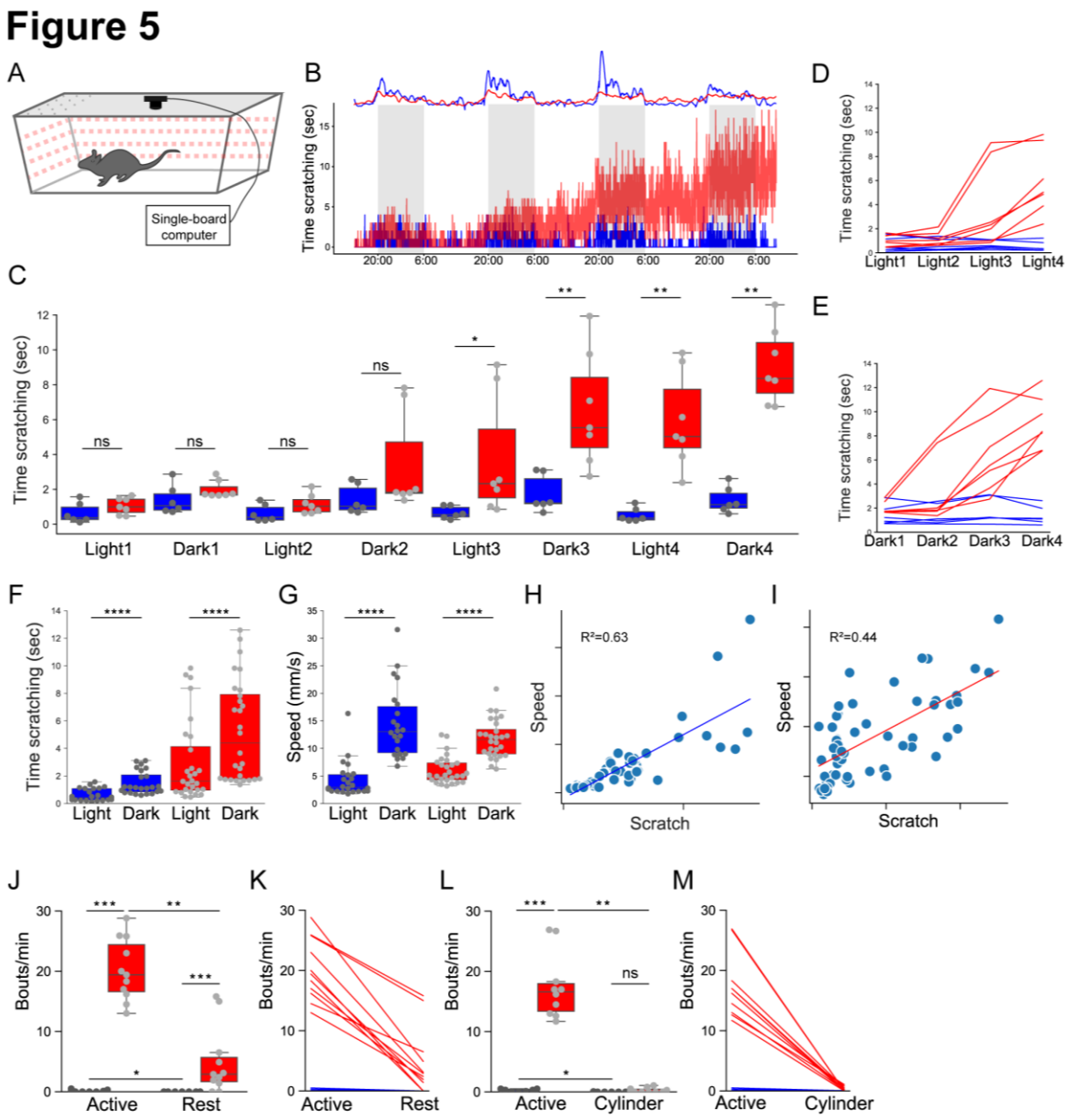

Figure 5. Spontaneous scratching in Ptf1a-ablated animals depends on locomotor activity.

A. Schematic representation of the setup used to record the activity of single housed control and Ptf1a-ablated mice continuously for several days.

B. Graphical representation of the time spent scratching as a function of time for ~90 hours of recording time. Top panel represents the average speed for control (blue, total average speed: 10.6±3.2 mm/s, n=6 mice) and Ptf1a-ablated (red, total average speed: 8.74±0.97 mm/s, n=7 mice) animals, two-sided Mann Whitney's unpaired u test: (st=19.0, p=0.83). Bottom panel represents the average scratching time per minute for control (blue, total average time: 0.98±0.25 seconds, n=6 mice) and for Ptf1a-ablated (red, total average time: 4.48±0.78 seconds, n=7 mice).

Two-sided Mann Whitney's unpaired u test: (st=0.0, **p=0.0034). Gray shadows represent the dark phase of the day cycle (light/dark cycle of 14/10 hours).

C. Quantification of scratching time in different light/dark phases for control (blue, n=6 mice) and Ptf1a-ablated (red, n=7mice) animals. No statistically significant differences: ns. Two-sided Mann Whitney's unpaired u test: *p<0.05, **p<0.01.

D. Time course change of mean scratching time in each light phase for individual control (blue, n=6 mice) and Ptf1a-ablated (red, n=7 mice) animals.

E. Time course change of mean scratching time in each dark phase for individual control (blue, n=6 mice) and Ptf1a-ablated (red, n=7 mice) animals.

F. Quantification of mean scratching time in control (blue, Light: 0.61±0.09 seconds, Dark: 1.48±0.17 seconds, n=6 mice) and Ptf1a-ablated (red, Light: 2.97± 0.56 seconds, Dark: 5.26± 0.68 seconds, n=7 mice) animals during light and dark phases. Two-sided Wilcoxon's signed-rank test, Control Light vs Dark (st=0.0, ****p=1.94×10^{-5}), Ptf1a-ablated Light vs Dark (st=0.0, ****p=4×10^{-6}).

G. Quantification of mean speed in control (blue, Light: 4.3±0.65 mm/s, Dark: 14.55±1.37 mm/s, n=6 mice) and Ptf1a-ablated (red, Light: 6.1±0.47 mm/s, Dark: 11.73±0.65 mm/s, n=7 mice) animals during light and dark phases. Two-sided Wilcoxon's signed-rank test, Control Light vs Dark (st=-4.1, ****p=4.01×10^{-5}), Ptf1a-ablated Light vs Dark (st= -4.6, ****p=4.23×10^{-6}).

H. Ordinary linear regression analysis model fitting for scratching and speed data of control animals during the whole study (n= 6 mice) [$F(1,46)=79.54$, $p=1.36 \times 10^{-10}$)].

I. Ordinary linear regression analysis model fitting for scratching and speed data of Ptf1a-ablated animals during the whole study (n= 7 mice) [$F(1,54)=43.12$, $p=2.08 \times 10^{-8}$)].

J. Quantification of scratching frequency in control (blue) and Ptf1a-ablated (red) animals at peak day in their home cages (Active) and 30 minutes after returning them to their respective racks (Rest). Control: active (0.12±0.05 bouts/min), rest (0±0 bouts/min), n=10 mice; Ablated: active (20.17±1.54 bouts/min), rest (4.9±1.67 bouts/min), n=11 mice. Two-sided Mann Whitney's unpaired u test, Active: (st=0.0, ***p=0.0001), Rest: (st=10.0, ***p=0.0005). Two-sided Wilcoxon's signed-rank test, Control: (st=0.0, *p=0.031), Ablated: (st=0.0, **p=0.003).

K. Individual mice representation of data in G, blue lines: control, red lines: Ptf1a-ablated animals.

L. Quantification of scratching frequency in control (blue) and Ptf1a-ablated (red) animals at peak day in their home cages (Active) and 1 hour later inside the startle response cylinder (Cylinder). Control: active (0.243±0.08 bouts/min), cylinder (0.013±0.01 bouts/min), n=7 mice; Ablated: active (17.39±1.71 bouts/min), cylinder (0.281±0.12 bouts/min), n=10 mice. Two-sided Mann Whitney's unpaired u test, Active: (st=0, ***p= 0.00074), Cylinder: (st= 22.5, ^{ns}p= 0.1898). Two-sided Wilcoxon's signed-rank test, Control: (st=1.0, *p= 0.045), Ablated: (st=0.0, **p= 0.0050).

M. Individual mice representation of data in I, blue lines: control, red lines: Ptf1a-ablated animals.

See also Figure S5.

Figure S5

A

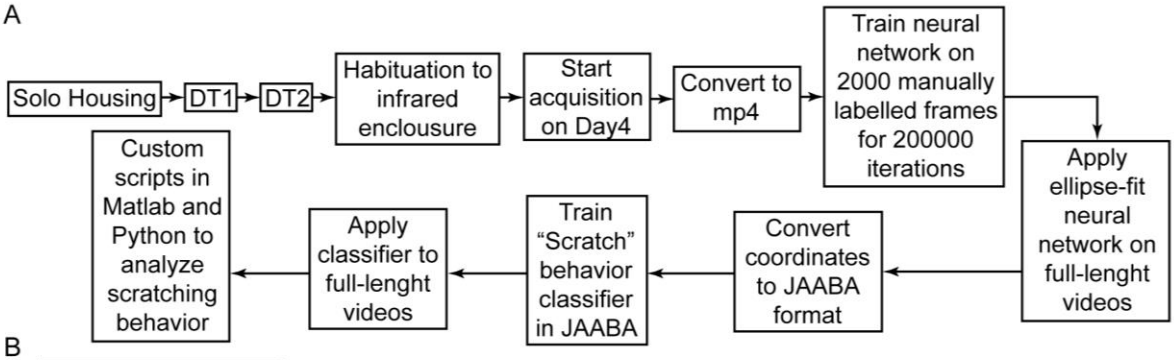

B

C

Ground Truth	Scratch Predicted	None Predicted
Scratch	251 (88.4%)	33 (11.6%)
None	153 (22.0%)	544 (78.0%)

D

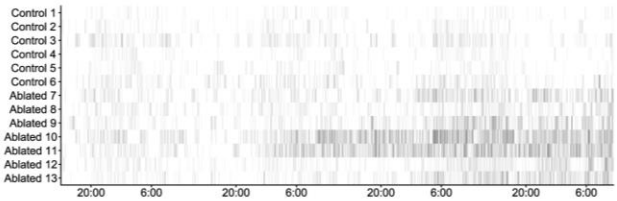

E

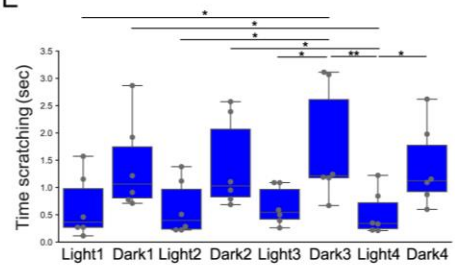

F

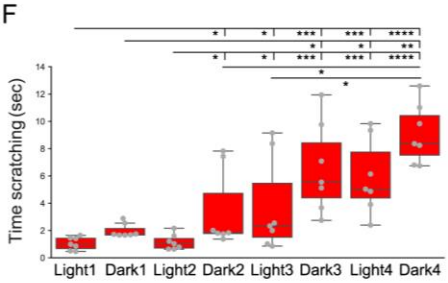

G

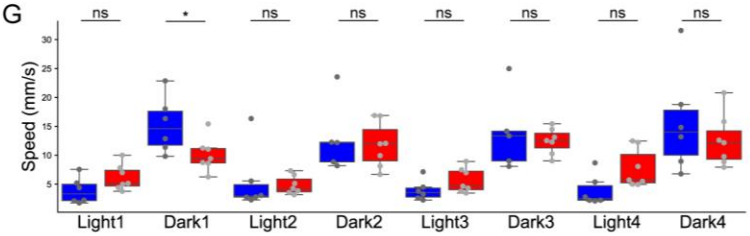

H

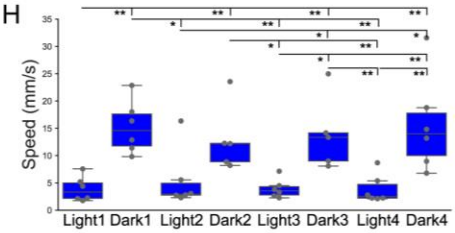

I

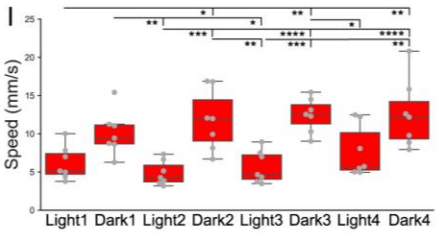

Figure S5. Overview and analysis of long-term naturalistic mouse behavior (related to Figure 5).

A. Protocol pipeline for acquisition, analysis and quantification of 90 hour data from mice in their home cages.

B. Representative images of the outcome from the neural network trained to identify, segment and fit an ellipse to mice.

C. JAABA classification scores in ground-truth mode.

D. Raster plot representation of individual scratch events for each control (n=6 mice) and Ptf1a-ablated (n=7 mice) animals during the whole ~90 hours of acquired video.

E. Quantification of scratching time in control animals (n=6 mice) during consecutive light/dark phases. One-way Kruskal-Wallis test followed by post hoc Fisher's least significance difference comparison: *$p<0.05$, **$p<0.01$.

F. Quantification of scratching time in Ptf1a-ablated animals (n=7 mice) during consecutive light/dark phases. One-way Kruskal-Wallis test followed by post hoc Fisher's least significance difference comparison: *$p<0.05$, **$p<0.01$, ***$p<0.001$, ****$p<0.0001$. Note: Y axis scale is different from the one in E.

G. Quantification of speed in different light/dark phases for control (blue, n=6 mice) and Ptf1a-ablated (red, n=7mice) animals. No statistically significant differences: ns. Two-sided Mann Whitney's unpaired u test: *$p<0.05$.

H. Quantification of speed in control animals (n=6 mice) during consecutive light/dark phases. One-way Kruskal-Wallis test followed by post hoc Fisher's least significance difference comparison: *$p<0.05$, **$p<0.01$.

I. Quantification of speed in Ptf1a-ablated animals (n=7 mice) during consecutive light/dark phases. One-way Kruskal-Wallis test followed by post hoc Fisher's least significance difference comparison: *$p<0.05$, **$p<0.01$, ***$p<0.001$, ****$p<0.0001$. Note: Y axis scale is different from the one in H.

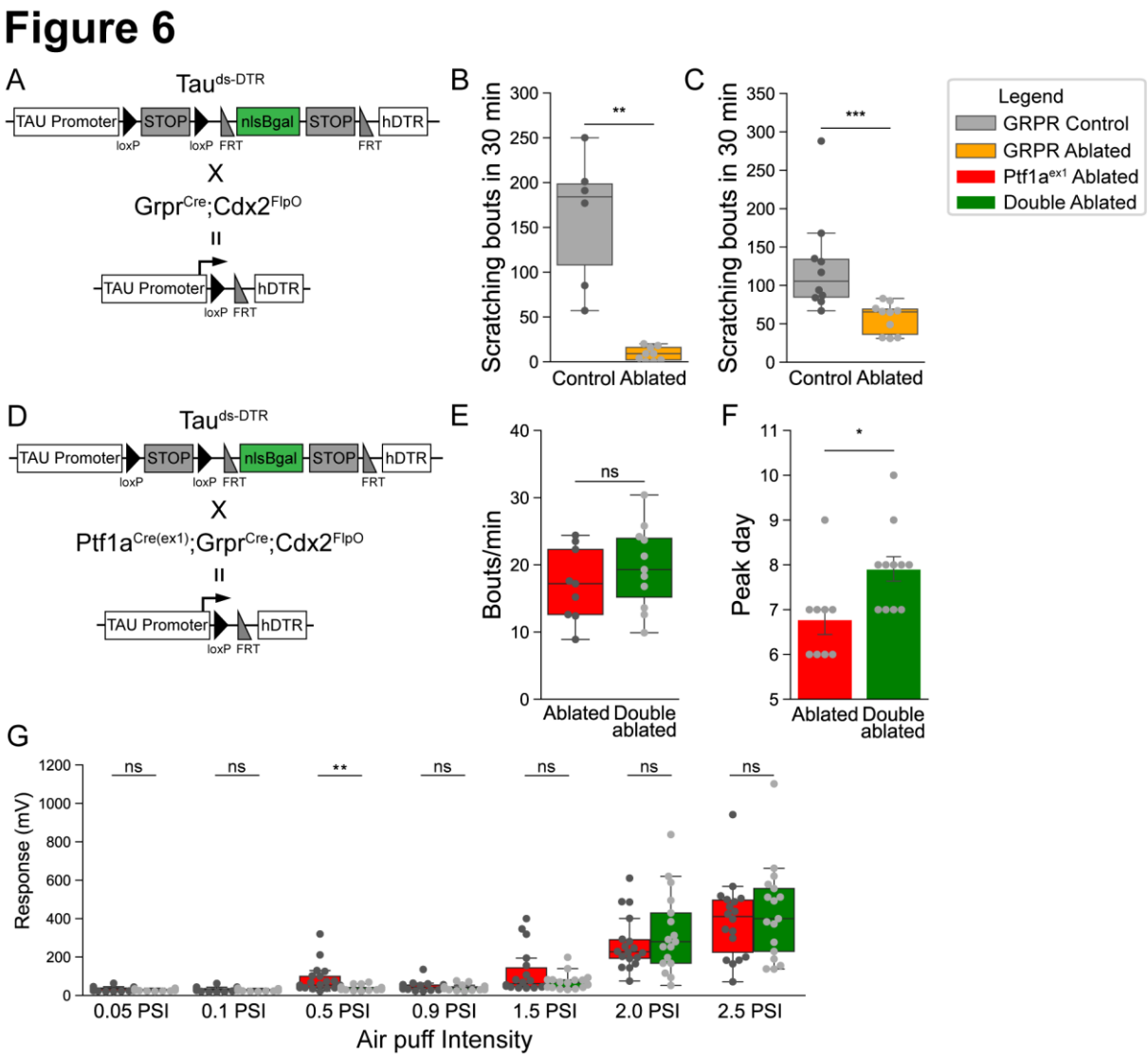

Figure 6. Ptf1a-ablation induced itch phenotype is mediated by GRPR neurons.

A. Schematic representation of genetic crosses for GRPR-ablation in the spinal cord.

B. Quantification of scratching bouts in control (grey) and GRPR-ablated (orange) animals after injection of chloroquine into the back. Control: 160.16±30.14 bouts, n=6 mice, Ablated: 8.66±2.6 bouts, n=9 mice. Two-sided Welch's t test, (st= 5.006, **p= 0.004).

C. Quantification of scratching bouts in control (grey) and GRPR-ablated (orange) animals after injection of compound 48/80 into the back. Control: 125±20.6 bouts, n=10 mice, Ablated: 57.5±6.33 bouts, n=10 mice. Two-sided Mann Whitney's u test, (st= 94.5, ***p= 0.00087).

D. Schematic representation of genetic crosses for Ptf1a- and GRPR- simultaneous ablation in the spinal cord.

E. Quantification of scratching frequency in Ptf1a-ablated (red) and Ptf1a;GRPR-ablated (green) animals in their home cages, at peak day after DT treatment. Ptf1a-ablated: 17.12±1.8 bouts/minute, n=9 mice, Ptf1a;GRPR-ablated: 19.63±1.87 bouts/minute, n=11 mice. Two-sided Student's unpaired t test, (st= -0.950, ^{ns}p= 0.354).

F. Quantification of time after DT1 in which Ptf1a-ablated (red) and Ptf1a;GRPR-ablated (green) animals reached maximum scratching frequency. Ptf1a-ablated: 6.7±0.32 days postDT, n=9 mice, Ptf1a;GRPR-ablated: 7.9±0.28 days postDT, n=11 mice. Two-sided Mann Whitney's u test, (st= 17.5, *p= 0.0122).

G. Quantification of the activity response elicited by air puffs of increasing intensity directed towards the back of Ptf1a-ablated (red) and Ptf1a;GRPR-ablated (green) animals. n = 17-21 animals per group and timepoint. Two-sided Mann Whitney's unpaired u test, 0.5 PSI: (st=271.0, **p=0.0016), rest: p > 0.05.

See also Figure S6.

Figure S6

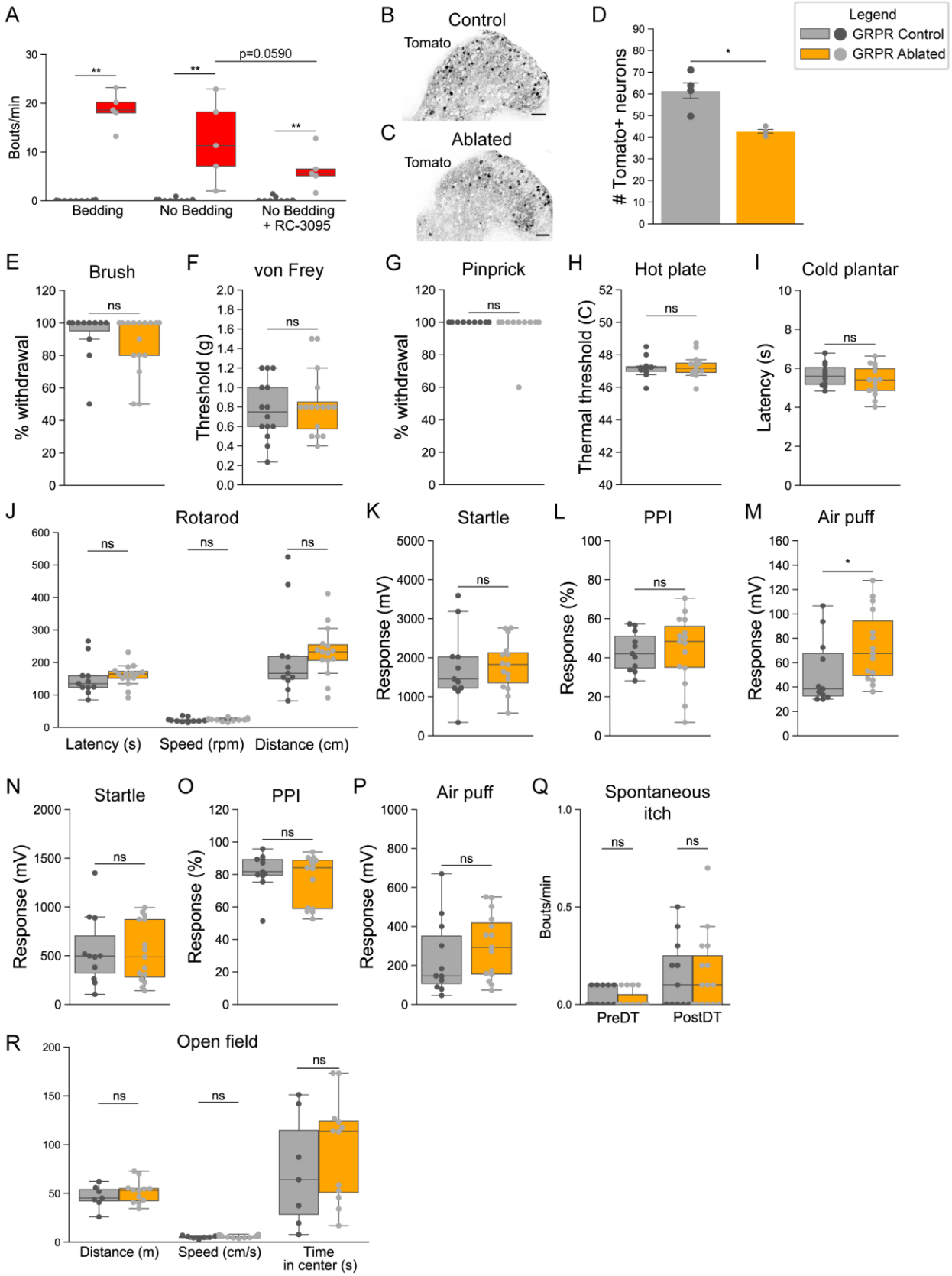
A
Bouts/min
**
**
p=0.0590
**
Bedding
No Bedding
No Bedding + RC-3095
B
Control
Tomato
C
Ablated
Tomato
D
Tomato+ neurons
*
Legend
GRPR Control
GRPR Ablated
E
Brush
% withdrawal
ns
F
von Frey
Threshold (g)
ns
G
Pinprick
% withdrawal
ns
H
Hot plate
Thermal threshold (C)
ns
I
Cold plantar
Latency (s)
ns
J
Rotarod
ns
ns
ns
Latency (s)
Speed (rpm)
Distance (cm)
K
Startle
Response (mV)
ns
L
PPI
Response (%)
ns
M
Air puff
Response (mV)
*
N
Startle
Response (mV)
ns
O
PPI
Response (%)
ns
P
Air puff
Response (mV)
ns
Q
Spontaneous itch
Bouts/min
ns
ns
PreDT
PostDT
R
Open field
ns
ns
ns
Distance (m)
Speed (cm/s)
Time in center (s)

Figure S6. GRPR-ablated animals behavioral characterization (related to Figure 6).

A. Quantification of GRPR antagonist RC-3095 effect on scratching frequency in control (blue) and Ptf1a-ablated (red) animals. Bedding: control (0.044±0.024 bouts/minute, n=9 mice), Ptf1a-ablated (18.64±1.63 bouts/minute, n=5 mice), No bedding: control (0.166±0.097 bouts/minute, n=9 mice), Ptf1a-ablated (12.3±3.75 bouts/minute, n=5 mice), No bedding + RC-3095: control (0.25±0.167 bouts/minute, n=9 mice), Ptf1a-ablated(6.32±1.82 bouts/minute, n=5 mice). Two-sided Mann Whitney's unpaired u test, Bedding: (st=0.0, **p=0.0022), No bedding: (st=0.0, **p=0.0026), No bedding + RC-2095: (st=0.0, **p=0.0023). Two-sided Wilcoxon signed rank paired test, Ablate No bedding-No bedding+RC-3095: (st=0.0, ^{ns}p=0.0590).

B-C. Representative images of adult thoracic spinal cord hemisection showing GRPR neurons expressing Tomato before (B) and two weeks after (C) diphtheria toxin delivery. Scale bar: 50 µm.

D. Quantification of the number of Tomato^{+} neurons in a dorsal hemisection of the spinal cord in control (darkgrey, 61.5±4.43 cells, n=4 mice) and GRPR-ablated (orange, 42.7±1.4 cells, n=3 mice) animals. Bars represent mean ± SEM. Two-sided Student's unpaired t test, (st=3.495, *p=0.017).

E. No differences in dynamic brush test between control (darkgrey, 92.72±4.7%, n=11 mice) and GRPR-ablated (orange, 87.5±4.42%, n=16 mice) animals 2 weeks after DT1. Two-sided Mann Whitney's unpaired u test, (st=104.0, ^{ns}p=0.376).

F. No differences in von Frey test between control (darkgrey, 0.77±0.08 g, n=14 mice) and GRPR-ablated (orange, 0.83±0.08, n=16 mice) animals 2 weeks after DT1. Two-sided Mann Whitney's unpaired u test, (st=104.0, ^{ns}p=0.751).

G. No differences in pinprick test between control (darkgrey, 100±0%, n=11 mice) and GRPR-ablated (orange, 97.5±2.5%, n=16 mice) animals 2 weeks after DT1. Two-sided Mann Whitney's unpaired u test, (st=93.5, ^{ns}p=0.451).

H. No differences in hot plate test between control (darkgrey, 47.2±0.19°C, n=11 mice) and GRPR-ablated (orange, 47.27±0.17°C, n=16 mice) animals 2 weeks after DT1. Two-sided Student's unpaired t test, (st=-0.27, ^{ns}p=0.78).

I. No differences in cold plantar test between control (darkgrey, 5.66±0.18s, n=11 mice) and GRPR-ablated (orange, 5.35±0.19s, n=15 mice) animals 2 weeks after DT1. Two-sided Student's unpaired t test, (st=1.11, ^{ns}p=0.277).

J. No differences in rotarod test between control (darkgrey, latency: 151.3±16.7s, speed: 22.88±1.97 rpm, distance: 218.37±41.48 cm, n=11 mice) and GRPR-ablated (orange, latency: 159.97±8.54s, speed: 24.06±1.04 rpm, distance: 232.66±20.32 cm, n=15 mice) animals 2 weeks after DT1. Two-sided Mann Whitney's unpaired u test, Latency: (st=54.5, ^{ns}p=0.1534), Speed: (st=54.5, ^{ns}p=0.1528), Distance: (st=54.5, ^{ns}p=0.1534).

K-M. No differences in tactile-acoustic startle response test between control (darkgrey, startle: 1756.52±281.93 mV, PPI: 43.13±3.04%, prepulse: 52.33±8.27 mV, n= mice) and GRPR-ablated (orange, startle: 1794.9±166.63 mV, PPI: 44.36±4.6%, prepulse: 73.3±7.55 mV, n= mice) animals

2 weeks after DT1. Two-sided Student's unpaired t test, Startle: (st=-0.124, ^{ns}p=0.90), PPI (st=-0.2065, ^{ns}p=0.84). Two-sided Mann Whitney's unpaired u test, Prepulse: (st=40.0, *p=0.029).

N-P. No differences in tactile-tactile startle response test between control (darkgrey, startle: 554.54±108.8 mV, PPI: 81.8±3.55%, prepulse: 240.78±59.31 mV, n=11 mice) and GRPR-ablated (orange, startle: 536.7±79.97 mV, PPI: 77.04±3.93%, prepulse: 299.29±42.76 mV, n=15 mice) animals 2 weeks after DT1. Two-sided Mann Whitney's unpaired u test, PPI: (st=90.0, ^{ns}p=0.716). Two-sided Student's unpaired t test, Startle: (st=0.135, ^{ns}p=0.89), Prepulse: (st=-0.822, ^{ns}p=0.419).

Q. Quantification of scratching frequency in control (darkgrey) and GRPR-ablated (orange) animals in their home cages, before and after DT treatment. Control (PreDT: 0.045±0.016 bouts/minute, n=11 mice, PostDT: 0.154±0.054 bouts/minute, n=11 mice), Ablated (PreDT: 0.026±0.012 bouts/minute, n=15 mice, PostDT: 0.16±0.05 bouts/minute, n=15 mice). Two-sided Mann Whitney u test, PreDT (st=98.0, ^{ns}p=0.345), PostDT (st=82.0, ^{ns}p=1.0).

R. No differences in open field test between control (darkgrey, distance: 46.52±4.45 m, speed: 5.17±0.5 cm/s, time in center: 72.75±21.57 s, n=7 mice) and GRPR-ablated (orange, distance: 51.6±3.35 m, speed: 5.74±0.37 cm/s, time in center: 95.8±15.23 s, n=12 mice) animals after DT. Two-sided Student's unpaired t test, Distance: (st=-0.917, ^{ns}p=0.37), Speed: (st=-0.918, ^{ns}p=0.37), Time in center: (st=-1.015, ^{ns}p=0.34).

Figure 7

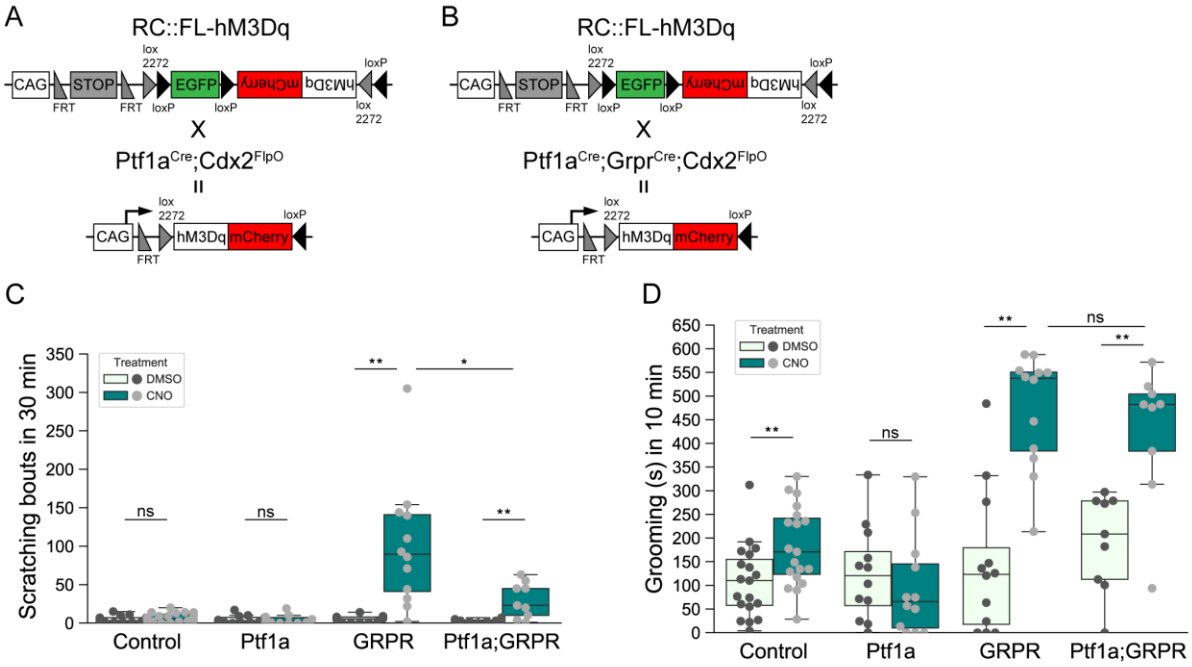

Figure 7. Ptf1a-activation inhibits GRPR-mediated itch.

A. Schematic representation of genetic crosses for DREADD-mediated activation of Ptf1a^{EX1} neurons in the spinal cord.

B. Schematic representation of genetic crosses for DREADD-mediated simultaneous activation of Ptf1a^{EX1} and GRPR neurons in the spinal cord.

C. CNO-mediated activation of GRPR neurons induces scratching (DMSO: 5.33±1.22 bouts vs CNO: 100.25±23.53 bouts, n=12 mice; Two-sided Student's paired t test, st=-3.99, **p=0.0021) which can be reduced through simultaneous activation of GRPR- and Ptf1a-derived neurons (DMSO: 3.33±0.67 bouts vs CNO: 29.55±7.66 bouts, n=9 mice; Two-sided Student's paired t test, st=-3.55, **p=0.0074; GRPRCNO: 100.25±23.53 bouts, n=12 mice vs Ptf1a;GRPRCNO: 29.55±7.66 bouts, n=9 mice, Two-sided Student's unpaired t test, st=2.85, *p=0.013). No differences are observed upon CNO administration to control (DMSO: 4.68±0.92 bouts vs CNO: 7.10±1.32 bouts, n=19 mice; Two-sided Wilcoxon's signed-rank test, st=58.0, ^{ns}p=0.24)) or Ptf1a animals (DMSO: 4.83±1.46 bouts vs CNO:4.83±1.63, n=12 mice; Two-sided Wilcoxon's signed-rank test, st=33.0, ^{ns}p=1.0) compared to the same animals treated with vehicle DMSO.

D. CNO-treated control animals show increased grooming (DMSO: 108.06±17.5 seconds vs CNO: 182.57±19.3 seconds, n=19 mice) which CNO-mediated activation of Ptf1a-derived neurons counteracts (DMSO: 124.73±28.45 seconds vs CNO: 96.45±30.78 seconds, n=12 mice; Two-sided Wilcoxon's signed-rank test, st=28.0, ^{ns}p=0.41). However, intense grooming induced by CNO-mediated activation of GRPR neurons (DMSO: 142.42±43.74 seconds vs CNO: 470.84±34.7 seconds, n=12 mice; Two-sided Wilcoxon's signed-rank test, st=1.0, **p=0.0033) is not compensated for by the concomitant activation of Ptf1a-derived neurons (DMSO:

192.33±34.24 seconds vs CNO: 425.4±48.6 seconds, n=9 mice; Two-sided Wilcoxon's signed-rank test, st=2.0, *p=0.017; GRPRCNO: 470.8±34.7 seconds, n=12 mice vs Ptf1a;GRPRCNO: 425.4±48.6 seconds, n=9 mice, Two-sided Mann Whitney's unpaired u test, st=69.0, ^{ns}p=0.303).

See also Figure S7.

Figure S7

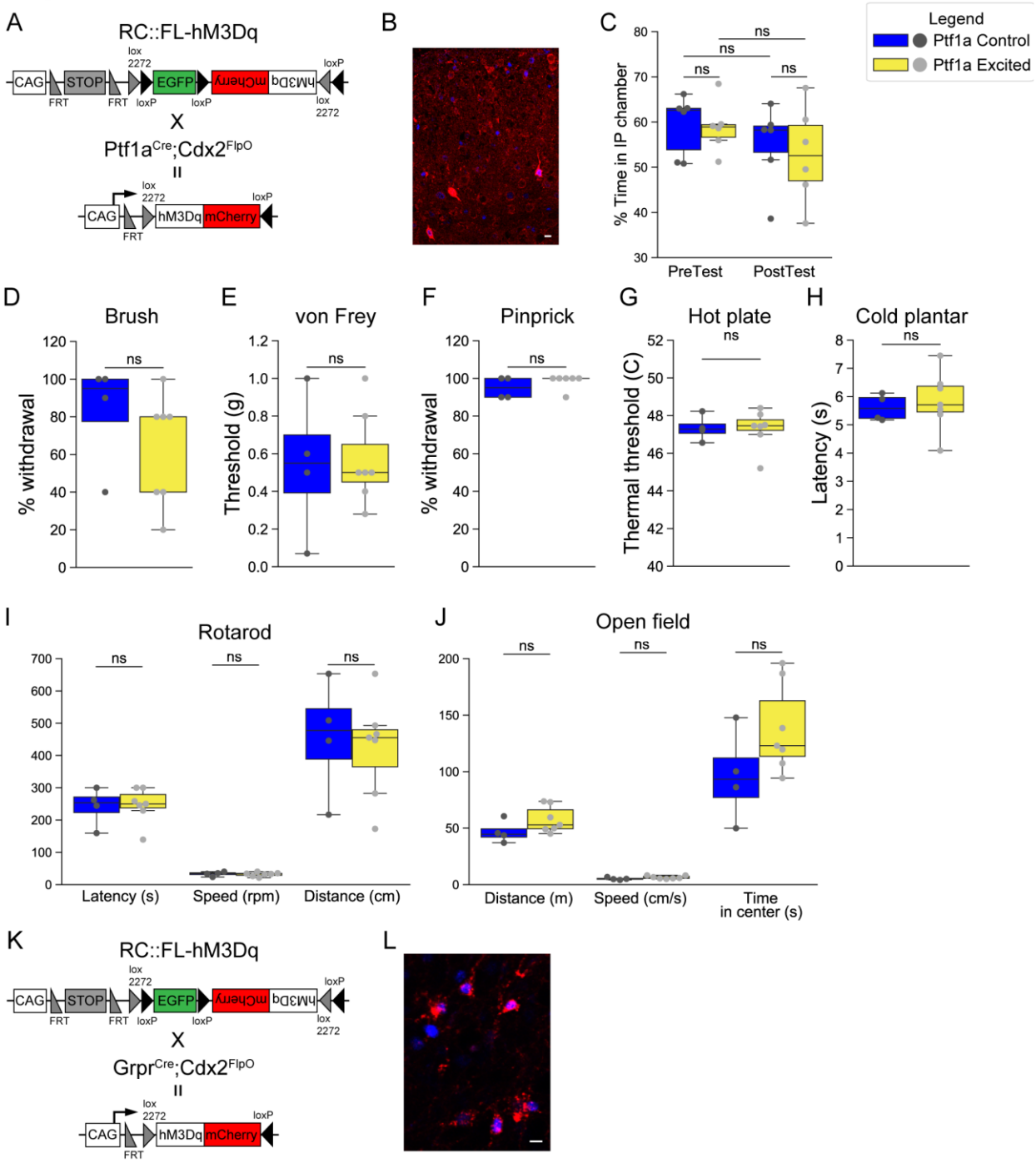

Figure S7. Ptf1a- and GRPR-activation through DREAD (related to Figure 7).

A. Schematic representation of genetic crosses for DREADD-mediated Ptf1a-derived neurons activation in the spinal cord.

B. Representative image of mCherry and cFos immunofluorescence in Ptf1a-activated neurons after CNO treatment. Scale bar: 10 µm.

C. CNO-mediated activation of Ptf1a-derived neurons does not have an effect on conditioned place preference. Control (blue, PreTest: 59.4±2.73%, PostTest: 55.03±3.66%, n=6 mice), Excited (green, PreTest: 58.8±2.3%, PostTest: 52.8±4.36%, n=6 mice). Two-sided Student's unpaired t test, PreTest: (st=0.16, ^{ns}p=0.87), PostTest: (st=0.38, ^{ns}p=0.70). Two-sided Student's paired t test, Control: (st=1.39, ^{ns}p=0.22), Excited: (st=2.31, ^{ns}p=0.069).

D. No differences in dynamic brush test between control (blue, 82.5±14.36%, n=4 mice) and Ptf1a-excited (green, 62.8±11.06%, n=7 mice) animals 30 minutes after CNO administration. Two-sided Mann Whitney's unpaired u test, (st=21.0, ^{ns}p=0.21).

E. No differences in von Frey test between control (blue, 0.54±0.19 g, n=4 mice) and Ptf1a-excited (green, 0.57±0.09, n=17 mice) animals 30 minutes after CNO administration. Two-sided Student's unpaired t test, (st=-0.14, ^{ns}p=0.89).

F. No differences in pinprick test between control (blue, 95±2.3%, n=4 mice) and Ptf1a-excited (green, 98.3±1.67%, n=6 mice) animals 30 minutes after CNO administration. Two-sided Mann Whitney's unpaired u test, (st=8.0, ^{ns}p=0.35).

G. No differences in hot plate test between control (blue, 47.33±0.34°C, n=4 mice) and Ptf1a-excited (green, 47.3±0.39°C, n=7 mice) animals 30 minutes after CNO administration. Two-sided Student's unpaired t test, (st=0.076, ^{ns}p=0.94).

H. No differences in cold plantar test between control (blue, 5.62±0.24s, n=4 mice) and Ptf1a-excited (green, 5.84±0.39s, n=7 mice) animals 30 minutes after CNO administration. Two-sided Student's unpaired t test, (st=-0.40, ^{ns}p=0.69).

I. No differences in rotarod test between control (blue, latency: 241.46±29.7 s, speed: 33.12±3.48 rpm, distance: 456.08±90.83 cm, n=4 mice) and Ptf1a-excited (green, latency: 246.1±20.5 s, speed: 31.67±2.32 rpm, distance: 424.35±58.5 cm, n=6 mice) animals 30 minutes after CNO administration. Two-sided Student's unpaired t test, Latency: (st=-0.13, ^{ns}p=0.89), Speed: (st=0.36, ^{ns}p=0.72), Distance: (st=0.31, ^{ns}p=0.76).

J. No differences in open field test between control (blue, distance: 46.68±4.93 m, speed: 5.19±0.55 cm/s, time in center: 96.01±20.26 s, n=4 mice) and Ptf1a-excited (green, distance: 57.56±4.4 m, speed: 6.4±0.49 cm/s, time in center: 137.95±14.77 s, n=7 mice) animals 30 minutes after CNO administration. Two-sided Student's unpaired t test, Distance: (st=-1.566, ^{ns}p=0.152), Speed: (st=-1.566, ^{ns}p=0.152), Time in center: (st=-1.7, ^{ns}p=0.125).

K. Schematic representation of genetic crosses for DREADD-mediated GRPR neurons activation in the spinal cord.

L. Representative image of mCherry and cFos immunofluorescence in GRPR-activated neurons after CNO treatment. Scale bar: 10 µm.

References

Abraira, V.E., Kuehn, E.D., Chirila, A.M., Springel, M.W., Toliver, A.A., Zimmerman, A.L., Orefice, L.L., Boyle, K.A., Bai, L., Song, B.J., et al. (2017). The Cellular and Synaptic Architecture of the Mechanosensory Dorsal Horn. Cell *168*, 295-310.e19.

Acton, D., Ren, X., Di Costanzo, S., Dalet, A., Bourane, S., Bertocchi, I., Eva, C., and Goulding, M. (2019). Spinal Neuropeptide Y1 Receptor-Expressing Neurons Form an Essential Excitatory Pathway for Mechanical Itch. Cell Reports *28*, 625-639.e6.

Alaynick, W.A., Jessell, T.M., and Pfaff, S.L. (2011). SnapShot: Spinal Cord Development. Cell *146*, 178-178.e1.

Aresh, B., Freitag, F.B., Perry, S., Blümel, E., Lau, J., Franck, M.C.M., and Lagerström, M.C. (2017). Spinal cord interneurons expressing the gastrin-releasing peptide receptor convey itch through VGLUT2-mediated signaling: PAIN *158*, 945–961.

Ashrafi, S., Betley, J.N., Comer, J.D., Brenner-Morton, S., Bar, V., Shimoda, Y., Watanabe, K., Peles, E., Jessell, T.M., and Kaltschmidt, J.A. (2014). Neuronal Ig/Caspr Recognition Promotes the Formation of Axoaxonic Synapses in Mouse Spinal Cord. Neuron *81*, 120–129.

Azim, E., Fink, A.J.P., and Jessell, T.M. (2014). Internal and External Feedback Circuits for Skilled Forelimb Movement. Cold Spring Harbor Symposia on Quantitative Biology *79*, 81–92.

Babayan, BM. and Conen, CS. (Eds.). (2019). Behavior matters [Special issue]. *Neuron, 104, 1,* p1-176.

Bardoni, R., Takazawa, T., Tong, C.-K., Choudhury, P., Scherrer, G., and MacDermott, A.B. (2013). Pre- and postsynaptic inhibitory control in the spinal cord dorsal horn: Inhibitory control in the dorsal horn. Annals of the New York Academy of Sciences *1279*, 90–96.

Bardoni, R., Barry, D.M., Li, H., Shen, K.-F., Jeffry, J., Yang, Q., Comitato, A., Li, Y.-Q., and Chen, Z.-F. (2018). Counter-stimuli Inhibit GRPR Neurons via GABAergic Signaling in the Spinal Cord. BioRxiv.

Betley, J.N., Wright, C.V.E., Kawaguchi, Y., Erdélyi, F., Szabó, G., Jessell, T.M., and Kaltschmidt, J.A. (2009). Stringent Specificity in the Construction of a GABAergic Presynaptic Inhibitory Circuit. Cell *139*, 161–174.

Borromeo, M.D., Meredith, D.M., Castro, D.S., Chang, J.C., Tung, K.C., Guillemot, F., and Johnson, J.E. (2014). A transcription factor network specifying inhibitory versus excitatory neurons in the dorsal spinal cord. Development *141*, 3102–3102.

Bourane, S., Duan, B., Koch, S.C., Dalet, A., Britz, O., Garcia-Campmany, L., Kim, E., Cheng, L., Ghosh, A., Ma, Q., et al. (2015a). Gate control of mechanical itch by a subpopulation of spinal cord interneurons. Science *350*, 550–554.

Bourane, S., Grossmann, K.S., Britz, O., Dalet, A., Del Barrio, M.G., Stam, F.J., Garcia-Campmany, L., Koch, S., and Goulding, M. (2015b). Identification of a Spinal Circuit for Light Touch and Fine Motor Control. Cell *160*, 503–515.

Bouvier, J., Caggiano, V., Leiras, R., Caldeira, V., Bellardita, C., Balueva, K., Fuchs, A., and Kiehn, O. (2015). Descending Command Neurons in the Brainstem that Halt Locomotion. Cell *163*, 1191–1203.

Brenner, D.S., Golden, J.P., and Gereau, R.W. (2012). A Novel Behavioral Assay for Measuring Cold Sensation in Mice. PLoS ONE *7*, e39765.

Britz, O., Zhang, J., Grossmann, K.S., Dyck, J., Kim, J.C., Dymecki, S., Gosgnach, S., and Goulding, M. (2015). A genetically defined asymmetry underlies the inhibitory control of flexor–extensor locomotor movements. ELife *4*.

Bröhl, D., Strehle, M., Wende, H., Hori, K., Bormuth, I., Nave, K.-A., Müller, T., and Birchmeier, C. (2008). A transcriptional network coordinately determines transmitter and peptidergic fate in the dorsal spinal cord. Developmental Biology *322*, 381–393.

Brownstone, R.M., and Chopek, J.W. (2018). Reticulospinal Systems for Tuning Motor Commands. Frontiers in Neural Circuits *12*.

Capelli, P., Pivetta, C., Soledad Esposito, M., and Arber, S. (2017). Locomotor speed control circuits in the caudal brainstem. Nature.

Chapman, E. and Tremblay, F. (2015), Scholarpedia, 10(3):7953

Cheng, L., Arata, A., Mizuguchi, R., Qian, Y., Karunaratne, A., Gray, P.A., Arata, S., Shirasawa, S., Bouchard, M., Luo, P., et al. (2004). Tlx3 and Tlx1 are post-mitotic selector genes determining glutamatergic over GABAergic cell fates. Nature Neuroscience *7*, 510–517.

Cheng, L., Samad, O.A., Xu, Y., Mizuguchi, R., Luo, P., Shirasawa, S., Goulding, M., and Ma, Q. (2005). Lbx1 and Tlx3 are opposing switches in determining GABAergic versus glutamatergic transmitter phenotypes. Nature Neuroscience *8*, 1510–1515.

Comer, J.D., Pan, F.C., Willet, S.G., Haldipur, P., Millen, K.J., Wright, C.V.E., and Kaltschmidt, J.A. (2015). Sensory and spinal inhibitory dorsal midline crossing is independent of Robo3. Frontiers in Neural Circuits *9*.

Cui, L., Miao, X., Liang, L., Abdus-Saboor, I., Olson, W., Fleming, M.S., Ma, M., Tao, Y.-X., and Luo, W. (2016). Identification of Early RET+ Deep Dorsal Spinal Cord Interneurons in Gating Pain. Neuron *91*, 1137–1153.

Delile, J., Rayon, T., Melchionda, M., Edwards, A., Briscoe, J., and Sagner, A. (2019). Single cell transcriptomics reveals spatial and temporal dynamics of gene expression in the developing mouse spinal cord. Development *146*, dev173807.

Detloff, M.R., Fisher, L.C., Deibert, R.J., and Basso, D.M. (2012). Acute and Chronic Tactile Sensory Testing after Spinal Cord Injury in Rats. Journal of Visualized Experiments.

Djouhri, L. (2016). Aδ-fiber low threshold mechanoreceptors innervating mammalian hairy skin: A review of their receptive, electrophysiological and cytochemical properties in relation to Aδ-fiber high threshold mechanoreceptors. Neuroscience & Biobehavioral Reviews *61*, 225–238.

Dong, X., and Dong, X. (2018). Peripheral and Central Mechanisms of Itch. Neuron *98*, 482–494.

Duan, B., Cheng, L., Bourane, S., Britz, O., Padilla, C., Garcia-Campmany, L., Krashes, M., Knowlton, W., Velasquez, T., Ren, X., et al. (2014). Identification of Spinal Circuits Transmitting and Gating Mechanical Pain. Cell *159*, 1417–1432.

Fink, A.J.P., Croce, K.R., Huang, Z.J., Abbott, L.F., Jessell, T.M., and Azim, E. (2014). Presynaptic inhibition of spinal sensory feedback ensures smooth movement. Nature *509*, 43–48.

Foster, E., Wildner, H., Tudeau, L., Haueter, S., Ralvenius, W.T., Jegen, M., Johannssen, H., Hösli, L., Haenraets, K., Ghanem, A., et al. (2015). Targeted Ablation, Silencing, and Activation Establish Glycinergic Dorsal Horn Neurons as Key Components of a Spinal Gate for Pain and Itch. Neuron *85*, 1289–1304.

François, A., Low, S.A., Sypek, E.I., Christensen, A.J., Sotoudeh, C., Beier, K.T., Ramakrishnan, C., Ritola, K.D., Sharif-Naeini, R., Deisseroth, K., et al. (2017). A Brainstem-Spinal Cord Inhibitory Circuit for Mechanical Pain Modulation by GABA and Enkephalins. Neuron 1–41.

Frost, W.N., Tian, L.-M., Hoppe, T.A., Mongeluzi, D.L., and Wang, J. (2003). A cellular mechanism for prepulse inhibition. Neuron *40*, 991–1001.

Fukuoka, M., Miyachi, Y., and Ikoma, A. (2013). Mechanically evoked itch in humans: Pain *154*, 897–904.

Geuther, B.Q., Deats, S.P., Fox, K.J., Murray, S.A., Braun, R.E., White, J.K., Chesler, E.J., Lutz, C.M., and Kumar, V. (2019). Robust mouse tracking in complex environments using neural networks. Communications Biology *2*.

Glasgow, S.M. (2005). Ptf1a determines GABAergic over glutamatergic neuronal cell fate in the spinal cord dorsal horn. Development *132*, 5461–5469.

Gross, M.K., Dottori, M., and Goulding, M. (2002). Lbx1 specifies somatosensory association interneurons in the dorsal spinal cord. Neuron *34*, 535–549.

Guo, Z., Zhao, C., Huang, M., Huang, T., Fan, M., Xie, Z., Chen, Y., Zhao, X., Xia, G., Geng, J., et al. (2012). Tlx1/3 and Ptf1a Control the Expression of Distinct Sets of Transmitter and Peptide Receptor Genes in the Developing Dorsal Spinal Cord. Journal of Neuroscience *32*, 8509–8520.

Hafenreffer, S. (1660). Nosodochion : in quo cutis, eique adhaerentium partium, affectus omnes, singulari methodo et cognoscendi et curandi fidelissime traduntur... (Ulm: Kühn).

Helms, A.W., and Johnson, J.E. (2003). Specification of dorsal spinal cord interneurons. Current Opinion in Neurobiology *13*, 42–49.

Hori, K., Cholewa-Waclaw, J., Nakada, Y., Glasgow, S.M., Masui, T., Henke, R.M., Wildner, H., Martarelli, B., Beres, T.M., Epstein, J.A., et al. (2008). A nonclassical bHLH Rbpj transcription factor complex is required for specification of GABAergic neurons independent of Notch signaling. Genes & Development *22*, 166–178.

Huang, M., Huang, T., Xiang, Y., Xie, Z., Chen, Y., Yan, R., Xu, J., and Cheng, L. (2008). Ptf1a, Lbx1 and Pax2 coordinate glycinergic and peptidergic transmitter phenotypes in dorsal spinal inhibitory neurons. Developmental Biology *322*, 394–405.

Huang, T., Lin, S.-H., Malewicz, N.M., Zhang, Y., Zhang, Y., Goulding, M., LaMotte, R.H., and Ma, Q. (2019). Identifying the pathways required for coping behaviours associated with sustained pain. Nature *565*, 86–90.

Hughes, D.I., Mackie, M., Nagy, G.G., Riddell, J.S., Maxwell, D.J., Szabo, G., Erdelyi, F., Veress, G., Szucs, P., Antal, M., et al. (2005). P boutons in lamina IX of the rodent spinal cord express high levels of glutamic acid decarboxylase-65 and originate from cells in deep medial dorsal horn. Proceedings of the National Academy of Sciences *102*, 9038–9043.

Ikoma, A., Handwerker, H., Miyachi, Y., and Schmelz, M. (2005). Electrically evoked itch in humans: Pain *113*, 148–154.

Juravle, G., Binsted, G., and Spence, C. (2017). Tactile suppression in goal-directed movement. Psychonomic Bulletin & Review *24*, 1060–1076.

Kabra, M., Robie, A.A., Rivera-Alba, M., Branson, S., and Branson, K. (2013). JAABA: interactive machine learning for automatic annotation of animal behavior. Nature Methods *10*, 64–67.

Kawaguchi, Y., Cooper, B., Gannon, M., Ray, M., MacDonald, R.J., and Wright, C.V.E. (2002). The role of the transcriptional regulator Ptf1a in converting intestinal to pancreatic progenitors. Nature Genetics *32*, 128–134.

Kini, S.P. (2011). The Impact of Pruritus on Quality of Life: The Skin Equivalent of Pain. Archives of Dermatology *147*, 1153.

Koch, S.C., Del Barrio, M.G., Dalet, A., Gatto, G., Günther, T., Zhang, J., Seidler, B., Saur, D., Schüle, R., and Goulding, M. (2017). RORβ Spinal Interneurons Gate Sensory Transmission during Locomotion to Secure a Fluid Walking Gait. Neuron *96*, 1419-1431.e5.

Koch, S.C., Acton, D., and Goulding, M. (2018). Spinal Circuits for Touch, Pain, and Itch. Annual Review of Physiology *80*, 189–217.

Lallemend, F., and Ernfors, P. (2012). Molecular interactions underlying the specification of sensory neurons. Trends in Neurosciences *35*, 373–381.

Li, Y., Qiu, Q., Watson, S.S., Schweitzer, R., and Johnson, R.L. (2010). Uncoupling skeletal and connective tissue patterning: conditional deletion in cartilage progenitors reveals cell-autonomous requirements for Lmx1b in dorsal-ventral limb patterning. Development *137*, 1181–1188.

Liang, H., Watson, C., and Paxinos, G. (2016). Terminations of reticulospinal fibers originating from the gigantocellular reticular formation in the mouse spinal cord. Brain Structure and Function *221*, 1623–1633.

Madisen, L., Zwingman, T.A., Sunkin, S.M., Oh, S.W., Zariwala, H.A., Gu, H., Ng, L.L., Palmiter, R.D., Hawrylycz, M.J., Jones, A.R., et al. (2010). A robust and high-throughput Cre reporting and characterization system for the whole mouse brain. Nature Neuroscience *13*, 133–140.

Madisen, L., Garner, A.R., Shimaoka, D., Chuong, A.S., Klapoetke, N.C., Li, L., van der Bourg, A., Niino, Y., Egolf, L., Monetti, C., et al. (2015). Transgenic Mice for Intersectional Targeting of Neural Sensors and Effectors with High Specificity and Performance. Neuron *85*, 942–958.

Mende, M., Fletcher, E.V., Belluardo, J.L., Pierce, J.P., Bommareddy, P.K., Weinrich, J.A., Kabir, Z.D., Schierberl, K.C., Pagiazitis, J.G., Mendelsohn, A.I., et al. (2016). Sensory-Derived Glutamate Regulates Presynaptic Inhibitory Terminals in Mouse Spinal Cord. Neuron *90*, 1189–1202.

Meredith, D.M., Masui, T., Swift, G.H., MacDonald, R.J., and Johnson, J.E. (2009). Multiple Transcriptional Mechanisms Control Ptf1a Levels during Neural Development Including Autoregulation by the PTF1-J Complex. The Journal of Neuroscience : The Official Journal of the Society for Neuroscience *29*, 11139–11148.

Mizuguchi, R., Kriks, S., Cordes, R., Gossler, A., Ma, Q., and Goulding, M. (2006). Ascl1 and Gsh1/2 control inhibitory and excitatory cell fate in spinal sensory interneurons. Nature Neuroscience *9*, 770–778.

Mollanazar, N.K., Sethi, M., Rodriguez, R.V., Nattkemper, L.A., Ramsey, F.V., Zhao, H., and Yosipovitch, G. (2016). Retrospective analysis of data from an itch center: Integrating validated tools in the electronic health record. Journal of the American Academy of Dermatology *75*, 842–844.

Mona, B., Uruena, A., Kollipara, R.K., Ma, Z., Borromeo, M.D., Chang, J.C., and Johnson, J.E. (2017). Repression by PRDM13 is critical for generating precision in neuronal identity. ELife *6*.

Moreno-López, Y., Olivares-Moreno, R., Cordero-Erausquin, M., and Rojas-Piloni, G. (2016). Sensorimotor Integration by Corticospinal System. Frontiers in Neuroanatomy *10*.

Müller, T., Brohmann, H., Pierani, A., Heppenstall, P.A., Lewin, G.R., Jessell, T.M., and Birchmeier, C. (2002). The homeodomain factor lbx1 distinguishes two major programs of neuronal differentiation in the dorsal spinal cord. Neuron *34*, 551–562.

Nakhai, H., Sel, S., Favor, J., Mendoza-Torres, L., Paulsen, F., Duncker, G.I.W., and Schmid, R.M. (2007). Ptf1a is essential for the differentiation of GABAergic and glycinergic amacrine cells and horizontal cells in the mouse retina. Development *134*, 1151–1160.

Oetjen, L.K., Mack, M.R., Feng, J., Whelan, T.M., Niu, H., Guo, C.J., Chen, S., Trier, A.M., Xu, A.Z., Tripathi, S.V., et al. (2017). Sensory Neurons Co-opt Classical Immune Signaling Pathways to Mediate Chronic Itch. Cell *171*, 217-228.e13.

Orefice, L.L., Zimmerman, A.L., Chirila, A.M., Sleboda, S.J., Head, J.P., and Ginty, D.D. (2016). Peripheral Mechanosensory Neuron Dysfunction Underlies Tactile and Behavioral Deficits in Mouse Models of ASDs. Cell *166*, 299–313.

Orefice, L.L., Mosko, J.R., Morency, D.T., Wells, M.F., Tasnim, A., Mozeika, S.M., Ye, M., Chirila, A.M., Emanuel, A.J., Rankin, G., et al. (2019). Targeting Peripheral Somatosensory Neurons to Improve Tactile-Related Phenotypes in ASD Models. Cell *178*, 867-886.e24.

Pagani, M., Albisetti, G.W., Sivakumar, N., Wildner, H., Santello, M., Johannssen, H.C., and Zeilhofer, H.U. (2019). How Gastrin-Releasing Peptide Opens the Spinal Gate for Itch. Neuron *103*, 102-117.e5.

Pan, H., Fatima, M., Li, A., Lee, H., Cai, W., Horwitz, L., Hor, C.C., Zaher, N., Cin, M., Slade, H., et al. (2019). Identification of a Spinal Circuit for Mechanical and Persistent Spontaneous Itch. Neuron.

Petitjean, H., Pawlowski, S.A., Fraine, S.L., Sharif, B., Hamad, D., Fatima, T., Berg, J., Brown, C.M., Jan, L.-Y., Ribeiro-da-Silva, A., et al. (2015). Dorsal Horn Parvalbumin Neurons Are Gate-Keepers of Touch-Evoked Pain after Nerve Injury. Cell Reports *13*, 1246–1257.

Poulet, J., and Hedwig, B. (2006). The cellular basis of a corollary discharge. Science *311*, 518–522.

Punnakkal, P., von Schoultz, C., Haenraets, K., Wildner, H., and Zeilhofer, H.U. (2014). Morphological, biophysical and synaptic properties of glutamatergic neurons of the mouse spinal dorsal horn: Glutamatergic neurons of the mouse dorsal horn. The Journal of Physiology *592*, 759–776.

Ross, S.E., Mardinly, A.R., McCord, A.E., Zurawski, J., Cohen, S., Jung, C., Hu, L., Mok, S.I., Shah, A., Savner, E.M., et al. (2010). Loss of Inhibitory Interneurons in the Dorsal Spinal Cord and Elevated Itch in Bhlhb5 Mutant Mice. Neuron *65*, 886–898.

Rudomin, P. (2009). In search of lost presynaptic inhibition. Experimental Brain Research *196*, 139–151.

Rudomin, P., and Schmidt, R.F. (1999). Presynaptic inhibition in the vertebrate spinal cord revisited. Experimental Brain Research. Experimentelle Hirnforschung. Expérimentation Cérébrale *129*, 1–37.

Russ, J.B., Verina, T., Comer, J.D., Comi, A.M., and Kaltschmidt, J.A. (2013). Corticospinal tract insult alters GABAergic circuitry in the mammalian spinal cord. Frontiers in Neural Circuits *7*.

Schut, C., Dalgard, F., Halvorsen, J., Gieler, U., Lien, L., Aragones, L., Poot, F., Jemec, G., Misery, L., Kemény, L., et al. (2019). Occurrence, Chronicity and Intensity of Itch in a Clinical Consecutive Sample of Patients with Skin Diseases: A Multi-centre Study in 13 European Countries. Acta Dermato Venereologica *99*, 146–151.

Sciolino, N.R., Plummer, N.W., Chen, Y.-W., Alexander, G.M., Robertson, S.D., Dudek, S.M., McElligott, Z.A., and Jensen, P. (2016). Recombinase-Dependent Mouse Lines for Chemogenetic Activation of Genetically Defined Cell Types. Cell Reports *15*, 2563–2573.

Seki, K., Perlmutter, S.I., and Fetz, E.E. (2003). Sensory input to primate spinal cord is presynaptically inhibited during voluntary movement. Nature Neuroscience *6*, 1309–1316.

Sorkin, L.S., and Puig, S. (1996). Neuronal model of tactile allodynia produced by spinal strychnine: effects of excitatory amino acid receptor antagonists and a mu-opiate receptor agonist. Pain *68*, 283–292.

Sorkin, L.S., Puig, S., and Jones, D.L. (1998). Spinal bicuculline produces hypersensitivity of dorsal horn neurons: effects of excitatory amino acid antagonists. Pain *77*, 181–190.

Sun, Y.-G., and Chen, Z.-F. (2007). A gastrin-releasing peptide receptor mediates the itch sensation in the spinal cord. Nature *448*, 700–703.

Sun, Y.-G., Zhao, Z.-Q., Meng, X.-L., Yin, J., Liu, X.-Y., and Chen, Z.-F. (2009). Cellular Basis of Itch Sensation. Science *325*, 1531–1534.

Takatoh, J., Nelson, A., Zhou, X., Bolton, M.M., Ehlers, M.D., Arenkiel, B.R., Mooney, R., and Wang, F. (2013). New Modules Are Added to Vibrissal Premotor Circuitry with the Emergence of Exploratory Whisking. Neuron *77*, 346–360.

Tripathi, R., Knusel, K.D., Ezaldein, H.H., Bordeaux, J.S., and Scott, J.F. (2019). The cost of an itch: A nationally representative retrospective cohort study of pruritus-associated health care expenditure in the United States. Journal of the American Academy of Dermatology *80*, 810–813.

Tripodi, M., Stepien, A.E., and Arber, S. (2011). Motor antagonism exposed by spatial segregation and timing of neurogenesis. Nature *479*, 61–66.

Ueno, M., Nakamura, Y., Li, J., Gu, Z., Niehaus, J., Maezawa, M., Crone, S.A., Goulding, M., Baccei, M.L., and Yoshida, Y. (2018). Corticospinal Circuits from the Sensory and Motor Cortices Differentially Regulate Skilled Movements through Distinct Spinal Interneurons. Cell Reports *23*, 1286-1300.e7.

Usoskin, D., Furlan, A., Islam, S., Abdo, H., Lönnerberg, P., Lou, D., Hjerling-Leffler, J., Haeggström, J., Kharchenko, O., Kharchenko, P.V., et al. (2015). Unbiased classification of sensory neuron types by large-scale single-cell RNA sequencing. Nature Neuroscience *18*, 145–153.

Voudouris, D., and Fiehler, K. (2017). Enhancement and suppression of tactile signals during reaching. Journal of Experimental Psychology: Human Perception and Performance *43*, 1238–1248.

Vrontou, S., Wong, A.M., Rau, K.K., Koerber, H.R., and Anderson, D.J. (2013). Genetic identification of C fibres that detect massage-like stroking of hairy skin in vivo. Nature *493*, 669–673.

Watson, A.H. (1992). Presynaptic modulation of sensory afferents in the invertebrate and vertebrate nervous system. Comparative Biochemistry and Physiology. Comparative Physiology *103*, 227–239.

Weisshaar, E., Szepietowski, J., Dalgard, F., Garcovich, S., Gieler, U., Giménez-Arnau, A., Lambert, J., Leslie, T., Mettang, T., Misery, L., et al. (2019). European S2k Guideline on Chronic Pruritus. Acta Dermato Venereologica *99*, 469–506.

Wickersham, I.R., Finke, S., Conzelmann, K.-K., and Callaway, E.M. (2006). Retrograde neuronal tracing with a deletion-mutant rabies virus. Nature Methods *4*, 47–49.

Wildner, H. (2006). dILA neurons in the dorsal spinal cord are the product of terminal and non-terminal asymmetric progenitor cell divisions, and require Mash1 for their development. Development *133*, 2105–2113.

Wildner, H., Das Gupta, R., Brohl, D., Heppenstall, P.A., Zeilhofer, H.U., and Birchmeier, C. (2013). Genome-Wide Expression Analysis of Ptf1a- and Ascl1-Deficient Mice Reveals New Markers for Distinct Dorsal Horn Interneuron Populations Contributing to Nociceptive Reflex Plasticity. Journal of Neuroscience *33*, 7299–7307.

Yosipovitch, G., and Bernhard, J.D. (2013). Chronic Pruritus. New England Journal of Medicine *368*, 1625–1634.

Zeilhofer, H.U., Wildner, H., and Yévenes, G.E. (2012). Fast Synaptic Inhibition in Spinal Sensory Processing and Pain Control. Physiological Reviews *92*, 193–235.

Zhang, J., Weinrich, J.A.P., Russ, J.B., Comer, J.D., Bommareddy, P.K., DiCasoli, R.J., Wright, C.V.E., Li, Y., van Roessel, P.J., and Kaltschmidt, J.A. (2017). A Role for Dystonia-Associated Genes in Spinal GABAergic Interneuron Circuitry. Cell Reports *21*, 666–678.

Zimmerman, A.L., Kovatsis, E.M., Pozsgai, R.Y., Tasnim, A., Zhang, Q., and Ginty, D.D. (2019). Distinct Modes of Presynaptic Inhibition of Cutaneous Afferents and Their Functions in Behavior. Neuron *102*, 420-434.e8.